Conjugate Point Equatorial Experiment (COPEX) Campaign in Brazil: Electrodynamics highlights on spread F development conditions and day-to-day variability

M. A. Abdu[1] , I. S. Batista[1], B. W. Reinisch[2] , J. R. de Souza[1] , J. H. A. Sobral[1], T. R. Pedersen[3] , A. F. Medeiros4[4] , N. J. Schuch[5] , E. R. de Paula[1]. K. M. Groves[3]

[1]Instituto Nacional de Pesquisas Espaciais, São José dos Campos, SP, Brasil.
[2]Center for Atmospheric Research, University of Massachusetts, Lowell, MA, USA
[3]Air Force Research Laboratory, AFRL/VSBXI, 29 Randolph Rd, Hanscom AFB, MA 01731-3010, USA.
[4]Universidade Federal de Campina Grande, PB, Brasil.
[5]Centro Regional Sul de Pesquisas Espaciais, INPE, Santa Maria, RS, Brasil.

Abstract:
A conjugate point equatorial experiment (COPEX) campaign was conducted during October - December 2002 period in Brazil, with the objective to investigate the equatorial spread F/plasma bubble irregularity (ESF) development conditions in terms of the electrodynamical state of the ionosphere along the magnetic flux tubes in which they occur. A network of instruments including digisondes, optical imagers, and GPS receivers, were deployed at magnetic conjugate and dip equatorial locations, in a geometry that permitted field line mapping of the conjugate E layers to dip equatorial F layer bottomside. We analyze in this paper the extensive digisonde data from the COPEX stations, complemented by limited all-sky imager conjugate point observations. The SUPIM (Sheffield University Plasmasphere-ionosphere Model) is used to assess the transequatorial winds (TEW) as inferred from the observed difference of hmF2 at the conjugate sites. New results and evidences on the ESF development conditions and the related ambient electrodynamic processes from this study can be highlighted as follows: 1) large scale bottomside wave structures/satellites traces at equator followed by their simultaneous appearance at conjugate sites are shown to be indicative of the ESF instability initiation; 2) the evening prereversal electric field enhancement (PRE)/vertical drift presents systematic control on the time delay in SF onset at off-equatorial sites indicative of the vertical bubble growth, under weak transequatorial wind; 3) the PRE presents large latitude/height gradient in the Brazilian sector; 4) conjugate point symmetry/asymmetry of large scale plasma depletions versus smaller scale structures are revealed; 5) while transequatorial winds seem to suppress ESF development in a case study, the medium term trend in the ESF seems to be controlled more by the variation in the PRE than in the TEW during the COPEX period. Competing influences of the evening vertical plasma drift in favoring the ESF development and that of the TEW in suppressing its growth are discussed presenting a perspective on the ESF day-to-day and medium term variabilities.

Keywords: Conjugate ionospheres; plasma bubble/spread F; vertical plasma drift; transequatorial wind; large scale wave structures; ESF day-to-day variability.

1. Introduction

Equatorial spread F/plasma bubble irregularities (ESF) development occurs under unique electrodynamical conditions of the ionosphere near sunset. The rapid uplift of the evening equatorial F layer is driven by an enhancement in the eastward electric field, widely known as the prereversal electric field enhancement (PRE), that arises from the dominating role of an F layer dynamo. The bottomside positive gradient region of the rapidly rising F layer becomes unstable to density perturbations leading to the growth of plasma depleted flux tubes/ plasma bubbles. A widely recognized fact is that the plasma bubbles are basically driven by the Rayleigh-Taylor interchange instability mechanism, operating on a "seed perturbation" at the bottomside density gradient region, and the lower density plasma of the F layer bottomside rises to the topside ionosphere in field aligned structures, under the action of strong polarization electric fields of the developing bubbles, as inferred directly or indirectly from measurements by different techniques (Hanson and Sanatani, 1973; Woodman and La Hoz, 1976; Tsunoda, 1981; Abdu et al., 1983a; Kelley, 1989; Fejer et al., 1999). The steep density gradient regions of the developing bubbles being conducive to the growth of secondary instabilities leads to a cascading process resulting in the formation of a wide spectrum of irregularities with scales sizes ranging from tens of centimeters to tens of kilometers (Haerendel et al., 1992). Thus in a flux tube aligned configuration the ESF structures extend in latitude depending upon their vertical growth/development above the dip equator. Based on the presently known theoretical and model simulation studies (for example, Zalesak et al., 1982; Sultan, 1996; Keskinen et al., 2003; see also, Abdu, 2001 for a review) the following interdependent factors of the ambient ionosphere–thermosphere system control such vertical growth: (1) the evening F layer height and the vertical plasma drift due to the prereversal electric field enhancement - PRE (Farley et al., 1970; Abdu et al., 1983b; Fejer et al., 1999) that are controlled by the thermospheric zonal wind (eastward in the evening) and the longitudinal/local time gradient in the integrated E layer conductivity near sunset (Rishbeth, 1971; Heelis et al., 1974), (2) development of a steep density gradient at the F layer bottomside where instability is initiated by seed perturbations (widely believed to be arising from gravity waves, see, for example, Fritts et al., 2008; Abdu et al., 2008), (3) the integrated Pedersen conductivity of the unstable flux tube which is controlled by thermospheric meridional/transequatorial winds, represented also by the symmetry/asymmetry conditions of the equatorial ionization anomaly (EIA) as proposed by Maruyama, (1988) and observationally investigated by various authors (e. g Valladares et al., 2001; Mendillo et al., 2001; Abdu et al., 2006b; Saito and Maruyama, 2006, Thampi et al., 2006). Sekar and Raghavarao (1995) have shown that the topside bubble growth and the zonal and vertical extents are dependent also on the background plasma densities and hence on the topside density gradients. The possible influence of a meridional wind from ETWA – Equatorial Temperature and Wind Anomaly- in the development of bottomside spread F has been discussed by Devasia et al. (2002) and Jyoti et al. (2004). The post sunset ESF occurrence is known to undergo variabilities at short-, day-to-day-, medium- and long- term scales. The long-term variation pattern is known to depend largely on the solar flux intensity. Its seasonal variation which is longitude dependent is understood in terms of the solar declination and the alignment of the solar terminator with magnetic meridian, i.e., the longitude

dependent magnetic declination angle (Abdu et al., 1981b; Tsunoda, 1985; Kil and Heelis, 1998; Burke et al., 2004; Su et al., 2008).

The pattern and causes of the ESF short-term and day-to-day variabilities, on the other hand, remain the least understood aspect of the ESF phenomenon. A better understanding of the nature of such variabilities is an important requirement toward developing any predictive capability on the ESF occurrence conditions. One aspect of the ESF variability appears to be interwoven in its relationship with the EIA (see, for example, Sridharan et al, 1994; Raghavarao et al. 1988; Abdu, 2001), while the broader question involves detailed analysis on the complex and competing roles of the above mentioned items 1 -3 in the ESF development. An important source of the ESF variability resides in what appears to be inherent in the nature of the seeding mechanism. In this respect it is under debate whether the seeding mechanism originates from a remote gravity wave source and/or local instability growth by other processes such as, for example, the wind driven instability of the bottomside F layer to serve as seed perturbation to topside bubble development, as proposed by Kudeki et al (2007), or the velocity shear mechanism at the F layer bottomside as proposed by Hysell and Kudeki (2004). The possibility of ESF initiation by electric field perturbation due to gravity waves winds in the E region has been discussed by Prakash (1999). Also under discussion is the possible role of a sporadic E layer instability mechanism for initiating the conditions for ESF development (Tsunoda, 2007; Casagrove and Tsunoda, 2002). More recently an important source of the ESF day-to-day variability has been shown to arise from planetary wave modulation of the evening prereversal enhancement in the zonal electric field (PRE)/vertical plasma drift (Abdu et al., 2006c). Ionosphere-magnetosphere coupling processes under magnetically disturbed conditions are also known to be an important source of the ESF variability (Sastri et al., 1997; Abdu, 1997; Abdu et al., 2003). A better understanding of the nature and causes of the variabilities in the ambient ionospheric electrodynamical parameters is a necessary requirement for further progress in this area. Motivated by the need to improve our understanding of the ESF day-to-day variability as related to some of the above factors, a conjugate point equatorial experiment (COPEX) campaign of approximately 2-month duration was conducted in Brazil during the October - December period of 2002. Data were collected on the vertical distribution of ionospheric electron density by Digisonde Portable Sounders (DPS-4s), airglow imageries using all-sky imagers, and GPS receivers for total electron content and L-band scintillation and irregularity zonal drift measurements.

This paper discusses the spread F development and the related symmetry/asymmetry conditions of the ambient ionospheric and electrodynamic parameters by analyzing the data from the equatorial and conjugate sites. The parameters analyzed include the signatures of the ESF in ionograms and of plasma density depletions in airglow all-sky imagers, the F layer electron density height distributions through their defining/critical parameters, hmF2 and foF2, and the evening F region vertical plasma drifts at the equatorial and conjugate sites, The conjugate point difference in F layer peak heights and the vertical drifts are used to infer the cross equatorial/meridional thermospheric winds and their day-to-day variability. The Sheffield University Plasmasphere-Ionosphere Model- SUPIM (Bailey and Balan, 1996) is used to evaluate the

transequatorial winds in terms of the hemispheric asymmetry in the EIA, that is, in terms of the conjugate point F layer peak heights, in this case. The overall analysis seeks to achieve a better understanding, and clarifications, on some major outstanding questions concerning the ESF onset and development characteristics, such as the role of large scale wave structures over the equator as precursor to spread F development, large and medium scale plasma irregularity structures and their conjugate point symmetry/asymmetry conditions, requirement of the evening prereversal enhancement in vertical drift for different conditions of bubble development (inferred by the differences in the observed time delays for spread F over off-equatorial sites), the role of the evening vertical drift in the ESF development as against the role of a transequatorial wind in suppressing such development, etc. Data are analyzed for magnetically quiet conditions and in the context of the relative roles of the different ambient parameters in influencing the spread F irregularity developments, and its day-to-day variability.

2. Experimental set up

The observing stations were located such that the conjugate E layers are field line mapped to the F layer peak, or to the F layer bottomside, over the magnetic equator, a geometry that can help investigate the possible effects on the bubble development process arising from changes in the field line integrated conductivity with associated changes in meridional/transequatorial winds. From the sketch of the magnetic field line - station geometry presented in **Fig. 1a** we note that the Brazilian territory in its central longitude region satisfies the required magnetic conjugacy conditions. The three selected locations are: Campo Grande (CG): 20° 26' 34" S; 54° 38' 47" W; dip:-22° 19' (southern conjugate point); Boa Vista (BV): 02° 49' 11" N, 60° 40' 24" W; dip: 22° (northern conjugate point); and Cachimbo (CX): 9° 28' 00" S, 54° 50' 00" W; dip: -4° 15'(near magnetic equator). We may note that the conjugate sites are somewhat equatorward of the Equatorial Ionization Anomaly (EIA) latitude which is nominally at ±15°-18° (dip angle: ±30°-36°). The map in **Fig. 1b** shows the geographic locations of the stations as well as the magnetic inclination and declination characteristics of the Brazilian region as specified in Table 1. Table 2 lists the network of instruments deployed at the different sites during the COPEX campaign, although the results to be presented here are based on the data source from a subset of the instruments consisting mainly of the DPS-4 sounders and the 630 nm all-sky imagers. The data collection by the DPS-4 (Reinisch, 1996) was at a cadence of 5 minutes during the night and 10 minutes during the day. The all-sky imaging data were collected at 5-minute intervals. Except for a few days of interruption over Boa Vista the digisonde data for all the stations covered all common days of the campaign interval that extended from the day 278 (October 05) to the day 344 (December 10) of the year 2002.

3. Presentation of the results

Some preliminary COPEX campaign results have previously been published and presented, e.g., Abdu et al. (2004), and Reinisch et al. (2004). The present paper and a companion paper by Sobral et al (2008, this issue) use the conjugate point digisonde and

all-sky optical imager data to address, respectively, issues related to (a) conjugate point ionospheric symmetry/asymmetry conditions related to the ESF mentioned earlier in the introduction, and (b) zonal plasma bubble irregularity drift velocities as obtained from the optical imageries and GPS spaced scintillation receivers and their theoretical evaluations, while the other COPEX results published more recently elsewhere concern (1) field line integrated conductivity effects as related to the connection between spread F development and Es layers at conjugate locations (Batista et al., 2008), (2) F2 peak parameters, drifts and spread F derived from Digisonde Ionograms for the COPEX Campaign in Brazil (McNamara et al., 2008) and (3) GPS L-band scintillations and ionospheric irregularity zonal drifts inferred at equatorial and low latitude regions (Muella et al, 2008). This paper concentrating on item (a) above, is organized in the remaining sections as follows: (3.1) General characteristics of the ESF irregularities at conjugate locations; (3.2) Evening vertical plasma drift (zonal electric field) and ESF development, (3.3) Symmetry/asymmetry in hmF2 and transequatorial winds (TEW), 3.4-Transequatorial winds and ESF, (3.5) Medium term trend in the transequatorial wind and evening vertical drift, (4) Discussion; and (5) Conclusions.

3.1 General characteristics of the ESF irregularities at the conjugate locations

The general characteristics of the ESF irregularities have been dealt extensively, for example, by Rastogi (1980), Abdu et al. (1981a), Kil and Heelis (1998), Su et al. (2008). **Fig. 2** shows the spread F initiation sequence at the three COPEX stations on the evening of October 09, 2002. The spread F onsets are marked by the appearance of oblique (off-vertical) traces (indicated by arrows) adjacent to the main F layer trace, indicating "large scale" wave structures in the bottomside electron density distribution. Their evolution into range-spread echo traces is captured with 5-minute resolution at all the three stations. The wave-structure (or its indication) first appears over Cachimbo (near the magnetic equator) in the ionogram at 2205 UT (1825 LT) which corresponds to an echo source located immediately west of the station (based on the virtual range and the echo location color code of the ionogram). Over the conjugate sites the first wave structure appears around 2245UT/1905LT (almost simultaneously within the uncertainty of the 5-minute observation cadence), close to North-East direction, by which time the trace over Cachimbo had evolved into a typical bottomside range spread structure (not shown here). The appearance of the first traces at the two conjugate stations indicative of a wave structure which is delayed with respect to such appearance over the equator has been verified to be a regular quiet day feature during the COPEX campaign period, and the ~ 40-minute delay observed in this case appears to represent a typical case of SF development sequence. We should note that an echo source separated in range by 50 km from the main vertical trace at 450 km (as in this example) corresponds to a horizontal separation of the reflection points by ~ 200 km. Observations of such oblique traces as precursors to SF have been reported before from single station observation over Fortaleza (Abdu et al., 1981a) and they seem to correspond to large scale wave structures similar to that discussed by Tsunoda (2008) from observations by the Altair incoherent scatter radar and ionosonde. The time delay in the appearance of the wave structures just described above has important implications on ESF development mechanism which will be discussed later.

Later in the night well-developed bubble structures drifted from the west into the all-sky imager field of view over Boa Vista and Campo Grande, nearly simultaneously. **Fig. 3** shows two sets of airglow depletion images, one for 0300 UT/2320 LT and another for 0330 UT/2350 LT, together with the corresponding ionogram spread F manifestations over the two stations. These bubble structures appear to have developed westward of the COPEX station probably initiated by a vertical drift increase in the preceding hours (near 01 UT), although the magnetic indices suggested a moderately quiet night. The imagers` field of view covers 1800 km in diameter at a reference altitude of 250 km, with maximum coverage extending to ~ ±20° of geomagnetic latitude. The higher latitude extremities of the depletions correspond to an equatorial apex height of >1000 km. The depletions in this figure thus correspond to well-developed bubble structures, and they drift eastward following their development at a westward longitude. We may note that the field aligned airglow depletions are almost completely symmetric over the two conjugate locations. All-sky imageries from previous conjugate point observations conducted in the Asia-Oceania longitude sector by Otsuka et al. (2002) that used significantly larger latitudinal separation than in the present experiment showed nearly perfect symmetry of the conjugate airglow depletions. The bubble zonal drift velocities in the present experiment are also symmetric over the conjugate sites as discussed in the companion paper by Sobral et al. (2008, this issue). L-band scintillation was present over Boa Vista and Campo Grande, with S_4 index attaining ~0.8 in discontinuous patches along all the monitored GPS satellites tracks (26), but with little scintillation over Cachimbo. The brighter background intensity of the 630 nm emission in these images indicates the equatorial ionization anomaly distribution. A faint circular feature (with reduced emission intensity) appears on the right side/eastern half of the image over Boa Vista which is absent over Campo Grande. The foF2 values (not shown here) are also asymmetric correspondingly.

The spread F traces in the ionograms over Boa Vista and Campo Grande corresponding to these optical images are shown on the left side of **Fig. 3**. The off-vertical spread F traces such as in the 0300 UT and 0330 UT ionograms are formed by coherent scatter returns from field aligned irregularities inside the depletions (bubbles) (Sales et al., 1996). Their appearance for frequencies f < foF2 indicates that the depletions extend to the bottom of the F layer. The spread F trace for f > fof2 indicates that the F2 depletion reaches at least up to hmF2, and likely into the topside. An increase in the top frequency of the spread F trace (often exceeding the foF2) indicates a decrease in the irregularity scale sizes detected by the digisonde. For f just above foF2, the F layer trace in the Campo Grande ionogram shows a negative slope (indicated by arrow) which is caused by the group retardation decreasing with increase of frequency, due to the underlying F2 layer. We may note that the irregularity strength and size distributions as indicated by the SF traces appear significantly asymmetric at the two stations, being less evolved over Campo Grande as compared to Boa Vista. We consider the range of spreading (in kilometers) as a qualitative measure of the spread F intensity for our discussion. The top scattered frequency of the F layer trace, indicative of the smallest scale size of the back-scattering irregularities, is also a measure of the ESF strength, which was perceivably smaller over CG than over BV conforming to the asymmetry. In view of the fact that the DPS-4 sounders and their antenna systems were identical at the conjugates stations the

presented asymmetry appears to arise from a difference in the SF characteristics at the two stations. This behavior contrasts with the near total symmetry observed in the optical images of the larger scale bubble structures (see also Sobral et al., 2008, this issue). There are many cases of such symmetry/asymmetry situations of the irregularity structures observed during the COPEX campaign. Further aspects on this question will be discussed in Section 4.

3.2 Characteristics of the evening vertical plasma drift (zonal electric field)

Vertical plasma drift velocity was calculated from the time rate of change of the F layer true heights, d(hF)/dt, at specific plasma frequencies as obtained from the SAO software of the Digisonde system (Reinisch, 1996; Khmyrov et al., 2008). The velocities so obtained are comparable with the vertical velocity calculated from the drift mode operation of the DPS-4 with the utilization of the Drift Explorer software (Abdu et al., 2006a; Kozlov and Paznukhov, 2008). These velocities correspond to the vertical displacement of the plasma densities responsible for the radio wave reflection. It has been shown from theoretical calculations (Bittencourt and Abdu, 1981) and experimental validation (Scali et al., 1995) that such velocities are identical to the vertical plasma drift velocities, for heights near and above 300 km where the recombination effect becomes negligible. Test was also done by comparing such velocities with the drift velocity from echo Doppler measurements obtained by the Digisonde drift explorer software (Abdu et al., 2006a) and in some cases (outside the COPEX data sets) with ion drift measurements by the Jicamarca incoherent radar (Bertoni et al., 2006). Usually for plasma frequencies above 4 MHz, but not when very close to the foF2, the results at different frequencies are generally comparable during evening hours when the F layer rises up under the prereversal enhancement in the zonal electric field. The results presented here consist of vertical drifts (Vz) measured at four plasma frequencies, 4 MHz, 5 MHz, 6 MHz, and 7 MHz. The Vz values obtained as the mean of the velocities at 4 and 5 MHz were compared with those obtained as the mean of the Vz values at 6 and 7 MHz. The two sets of the mean Vz values are found to be in general agreement. Therefore we have used both sets of Vz values in the analysis presented here.

Fig. 4 presents mass plots of vertical drifts over the three stations for all days of the COPEX campaign. The mean of all the Vz values are shown by the thick solid curve. Here we focus on the characteristics of the evening prereversal enhancement (PRE) in the vertical drift. The peak in the PRE has a mean value of 52 m/s over Cachimbo. Over Boa Vista and Campo Grande the velocities are significantly smaller, 20 m/s and 26 m/s, respectively. The prereversal enhancement peaks at ~1850 LT (2230 UT) at all the stations. Interesting characteristics of the PRE in these results are (a) the significant decrease of its intensity over the conjugate sites as compared to that over the equatorial site, and (b) a noticeable asymmetry in the intensity at the conjugate sites. Based on considerations of field line mapping of large scale electric fields the variation with latitude of the prereversal electric field as seen in this result corresponds to a height variation in the equatorial plane. Thus we note a significant decrease of the evening zonal electric field with height. The mean pattern shows a zonal electric field of ~1.2

mV/m, corresponding to a vertical drift of ~52 m/s, at a reference height of 450 km, which decreased to about half its value at ~650 km, the field line apex height for conjugate F layer bottomside at 350 km. (This decrease is less by 8% if we correct for the magnetic field inclination of 22° of the conjugate sites). Such negative height gradient of the evening zonal electric field has been observed by the Jicamarca radar for solar minimum flux levels (see for example, Pingree and Fejer, 1987). For F10.7 ≈150, identical to the mean flux values representing the COPEX campaign period, the available Jicamarca measurements (Bela Fejer, private communication) indicates a slower decrease rate with altitude of the evening vertical drift. This would suggest the existence of a significant longitudinal variation in the vertical gradient of the evening zonal electric field between Jicamarca and the COPEX stations, which needs to be investigated further. An asymmetry in the PRE amplitude between the two conjugate sites can be noted, the amplitude over CG being larger than over BV. This would indicate the presence of an average northward transequatorial wind during the COPEX period, the details of which will be discussed later.

3.2.1 Evening vertical drift enhancement and spread F development

The most important prerequisite for the generation of the postsunset spread F/plasma bubble irregularities is the uplift of the evening F layer due to the prereversal enhancement in the zonal (eastward) electric field (Farley, et al., 1970; Abdu et al., 1983b; Fejer et al., 1999). It is known that ambient conditions other than the PRE (such as those mentioned earlier) have roles to play in the control of the SF development. Below we will first examine the different aspects of the control of SF generation by the PRE. Some aspects on the evening prereversal vertical drift for spread F occurrence/non occurrence conditions over the equatorial site, Cachimbo, have been briefly presented in a paper by McNamara et al. (2008) and will not be discussed here. Below we will present the results of an analysis of the vertical drift over Cachimbo as well as over the two conjugate stations as a function of the spread F onset/occurrence local times at the latter two stations and at a southern low latitude site Cachoeira Paulista (dip angle: -33.7°). Possible influences of the transequatorial winds on the ESF development will also be discussed in this and subsequent sections.

Fig. 5 presents in four panels the mean V_z values representative of the days sorted out on considerations of systematic increase in time delays for SF occurrence at latitudes farther away from the dip equator. In this context we have included also in the analysis the Cachoeira Paulista (CP) site that is not aligned in magnetic meridian with the COPEX stations, and is located at higher magnetic latitude than the southern conjugate site Campo Grande. We consider here (as also pointed out earlier) that the vertical growth of the flux tube aligned plasma depletions over the equator, with the associated smaller scale structures, is responsible for the latitudinal extension of the spread F so that its occurrence over CP (as over the conjugate sites) can be considered to indicate the bubble vertical extension to the equatorial apex height of the field line that maps to the F layer bottomside over these stations (see also, Abdu et al., 1983a). The average ΣKp values corresponding to the sorted group of days are also shown in these panels. We may point out that in the evening and early night hours (and whenever the F layer height

is > 300 km, in general) the V_z values do represent realistic vertical drift. Based on the flux tube aligned bubble development just stated above the spread F occurrence at early post sunset local times (before 20 LT) over Cachoeira Paulista corresponds to rather fast vertical bubble rise velocities (>100 m/s) over the equator. Any effect from possible eastward drift of the bubble on the vertical velocity so estimated is expected to be small as discussed by Abdu et al. (1983b). The mean Vz variations corresponding to all such cases observed during the period are plotted for the three COPEX stations in panel 1 of **Fig. 5.** The Vzp over Cachimbo (magnetic equator) for this case is ~ 62 m/s. A second group of SF events occurring at and before 22 LT over CP is represented by the mean Vz variations shown in panel 2 of this figure. In this case the mean Vzp (over Cachimbo) is only slightly smaller, being 59 m/s. The results in panel 3 of **Fig. 5** show the case of SF not occurring till midnight over CP, which signifies that the vertical bubble growth over the equator did not attain till midnight an apex altitude of 900 km that is field line mapped to the bottomside F region over CP. The Vzp over Cachimbo for this case is around 35 m/s. The field line apex height for Campo Grande bottomside F region is ~ 650 km. For the cases of post sunset spread F not occurring over Campo Grande the mean Vz variation is shown in panel 4 of **Fig.5**. The value of Vzp for this case is 30 m/s which suggests that bubble vertical growth to ~650 km could be possible when the prereversal vertical drift is higher than this value. During the campaign period there were only two non spread F nights over Cachimbo (and all other stations). For those cases the mean Vzp (not shown here) was just 22 m/s, which can be considered to be the threshold minimum below which bottomside spread F did not occur over the equator. We note thus that the average Vzp presents a trend suggesting its systematic control on the spread F development, with the lowest Vzp (22 m/s) for the case of SF totally absent to the highest Vzp (~ 60 m/s) for an early SF occurrence over CP corresponding to a rapid (>100 m/s) vertical growth of the bubble over the equator. We may point out that the average PRE amplitudes over the conjugate sites were significantly smaller than over the equator and their asymmetry suggested the presence of a generally weak, and northward, transequatorial wind in the F layer bottomside, in all the cases considered above (as in Fig. 4). It is relevant to mention here that threshold conditions on the evening prereversal vertical drift for UHF and L-band scintillation occurrence in the Peruvian sector have been discussed by Anderson et al. (2004). We note further in Fig. 5 that the ΣKp values given in each of the panels present a systematic increase with decreasing evening vertical drift velocities, when at the same time the pre sunrise vertical drift presented a systematic increase. This point will be discussed later in Section 4.

3.3 Transequatorial winds from inter-hemispheric symmetry/asymmetry in hmF2

In the absence of plasma transport by meridional wind and electric field the F layer peak electron density occurs at a height h_0 where a balance between recombination and diffusion prevails (Rishbeth et al., 1978). Depending upon the magnetic field inclination a horizontal meridional wind (as well as a zonal electric field) can cause upward or downward displacement of the F layer with respect to h_0 producing the observed F layer peak height, hmF2. In the presence of a transequatorial wind hmF2 increases in the upwind hemisphere while it decreases in the downwind hemisphere. On the other hand any vertical displacement of the F layer due to large-scale zonal electric fields (such as

from the E and F layer dynamo) should be equal at the conjugate locations. In this way a difference in the hmF2 (ΔhmF2) observed between two magnetically conjugate locations is a good indicator of the sum of the meridional winds at the two locations. The relationship between the ΔhmF2 from conjugate stations and transequatorial winds has been studied by Bittencourt and Sahai (1978) using a tropical F region computational model. In the present investigation we have used the SUPIM code (Sheffield University Plasmasphere-Ionosphere Model, Bailey and Balan, 1996) to quantify the connection between the ΔhmF2 and the transequatorial wind for the COPEX conjugate stations as a function of UT (UT = LT + 3.6 hours). A methodology to calculate the equatorial zonal electric field and low latitude magnetic meridional winds based on hmF2 and foF2 over equatorial and low latitude ionosphere by the use of the SUPIM code has been discussed by Souza et al. (2000). The modeling results presented in **Fig. 6** show in the lower panel the $\Delta hmF2_{(CG\text{-}BV)}$, that is, hmF2(Campo Grande) – hmF2(Boa Vista) as modeled using the SUPIM code in which the HWM93 wind (Hedin et al., 1996) was one of the controlling input parameters. The zonal electric field, the other critical input parameter to the SUPIM, was based on the Scherliess and Fejer (1999) model that was modified by replacing the evening vertical drift with that calculated from the COPEX Digisonde data (see also, Medeiros et al., 1997). The calculation was done for conditions representative of October 2002. The sum of the meridional winds at the northern and southern conjugate stations, $U^N + U^S$, representative of this period, according to the HWM93 (that yielded the above $\Delta hmF2_{(CG\text{-}BV)}$) is also shown in the lower panel of **Fig. 6**. Positive (negative) $\Delta hmF2_{(CG\text{-}BV)}$ indicates northward (southward) transequatorial wind (TEW). The TEW is normally northward during much of the daytime and near midnight during this period (in October) in the model which is in general agreement with the observational results presented here, in Fig. 7 and in Fig. 8 (to be discussed below). The model results show that a magnitude of 1 kilometer in the $\Delta hmF2_{(CG\text{-}BV)}$ corresponds on an average to a TEW of 1 m/s and their ratio does not remain constant. The ratio of a change in $\Delta hmF2_{(CG\text{-}BV)}$ (in km) to a causative change in TEW (in m/s), that is, $d(\Delta hmF2_{(CG\text{-}BV)})/d(U^N + U^S)$ as calculated by the SUPIM for the same period is plotted in the top panel of **Fig. 6**. We may note that this value varies around unity as a function time for most of the daytime with slightly higher values during night hours. This information on the coefficient, $d(\Delta hmF2)/d(U_S + U_N)$, is useful for quantifying any conjugate point difference in hmF2 in terms of its driving tans-equatorial winds vis-à-vis implications on possible ESF development arising there from. (The day-to-day variations and medium term trends in ΔhmF2 and possible implications on SF will be discussed in Section 3. 5).

Fig. 7 (lower panel) presents a mass plot of all the observed $\Delta hmF2_{(CG\ -\ BV)}$ values during the entire campaign period as a function of UT. The mean of these curves with the standard deviations is shown separately (top panel, green curve) which presents a dominant diurnal oscillation superimposed by a less significant semi-diurnal oscillation. The north direction is upward (as in Fig. 6) indicated by an arrow. During most of the daytime (from ~06 to 16 LT) the COPEX average $\Delta hmF2_{(CG\ -\ BV)}$ suggests a TEW directed northward, whereas it tends to be southward in the presunrise (near 03 LT) and evening (around 18 LT) hours. For this case as well the $\Delta hmF2_{(CG\ -\ BV)}$ parameter was modeled by the SUPIM as an average pattern representative of the entire campaign

period. The results represented by the blue curve in the top panel show general agreement with the mean curve of the observational data. However, some disagreement is present at local times around midnight (03 UT and around midday (15 UT) when the modeled $\Delta hmF2_{(CG - BV)}$ are close to, or exceed, the upper limit of the SD (standard deviation) bars of observed values. The TEW according to the HWM93 that was used in the SUPIM calculation is plotted as the orange curve in the top panel. We may note that the variations in the two parameters are not in-phase. In other words, the relationship between the two quantities, the TEW (according to the HWM93) and the ΔhmF2 (that resulted from the calculation), representing the average conditions of the entire period, vary with local time in much the same way as they did in the example for October shown in **Fig. 6** (lower panel). The extent to which the TEW requires modification to obtain a more perfect agreement between the modeled and measured $\Delta hmF2_{(CG-BV)}$ will give a better idea as to how well the HWM93 represents the horizontal meridional wind pattern over Brazil during the COPEX period. Such an effort is in progress. Discrepancy between conjugate F layer base heights (h'F) as modeled by including the HWM93 and that obtained from observations has recently been reported by Maruyama et al. (2007) for Asian longitudes.

We note large day-to-day variability in the transequatorial winds (Fig. 7, lower panel). Different groups of quiet days were considered separately to verify the presence of any medium term variation in the diurnal pattern of these winds. Examples for a few quietest days of October and similar days in December are presented in **Fig. 8** in which both the $\Delta hmF2_{(CG - BV)}$ and $\Delta foF2_{(CG - BV)}$ variations are shown. The diurnal pattern that indicates northward directed TEW (during most of the daytime and near midnight) support the model results of Fig. 6 and 7. In the left panels we note that the ΔhmF2 indicates an increasingly more northward TEW from October to December, which might be due to the increase in the solar declination angle, with the sub-solar point for the thermospheric UV absorption moving well into the southern hemisphere towards the later part of the COPEX campaign period. The predominantly northward winds seem to be responsible for a significant decrease in the hmF2 over BV for most of the time as verified from the data (not shown here)**.** The corresponding $\Delta foF2_{(CG - BV)}$ plots in the right panels (**Fig. 8**) highlight, as the main point, a generally negative ΔfoF2 which intensifies during most of the night hours in December, which is a reflection of an increase of foF2 over Boa Vista at those hours (not shown here). This result suggests that a northward wind over Boa Vista in the night, which in this case is part of a transequatorial system, brings plasma down along the field lines, (apparently at a rate faster than the recombination rate), contributing to the increase of the foF2 over this station. On the other hand, during daytime we see a different picture. In December, when the transequatorial wind is more intense than in October, the $\Delta foF2_{(CG - BV)}$ did not show any correspondingly significant increase, which may be attributed to the influences from daytime dynamical/electrodynamical and photochemical processes. In fact the daytime foF2 values at both stations (not shown here) were less in December than in October, which would suggest that the equatorial anomaly fountain might be somewhat weaker during these December days than it was in October. This fact, even in the presence of an asymmetric ion production rates at the conjugate sites with the CG being much closer to the sub solar point than BV in December, appears to have contributed to a reduction of

the $\Delta foF2_{(CG-BV)}$ values in December as compared to October in Fig. 8. Further analysis of this problem could lead to a better understanding of the seasonal features in the equatorial fountain/anomaly vis-a-vis the possible role of transequatorial winds in such features.

3.4- Transequatorial winds and ESF

We may note that the larger southward TEW (represented by the larger negative ΔhmF2) that dominated the evening hours of the October quiet days was almost totally absent during the December interval (Fig. 8). A potential effect on ESF generation arising from such a change in the evening wind direction is an interesting possibility that needs to be investigated (see the discussion section). A transequatorial wind, whether directed northward or southward has the potential to suppress the post sunset ESF (e.g., Maruyama 1988; Abdu, 1997; Abdu et al., 2006b). This point can be addressed in terms of statistical as well as on a case study basis. We will here examine some specific cases in the COPEX data set which seem to provide evidence of ESF suppression by the transequatorial wind. In the example in **Fig. 9a** we present the evening vertical drift (due to the PRE) over Cachimbo, Boa Vista, and Campo Grande. Three days of October 10, 12 and 23, when the Vz variations during the PRE are very much identical over Cachimbo are plotted in the left panel. The corresponding Vz variations over the conjugate stations (middle and right panels) show significantly reduced Vz amplitude like in the statistical plot of **Fig. 4**. On two days, i.e., October 10 and 12, the evening Vz variations are nearly identical/symmetrical and are significantly larger (35 m/s) at the two conjugate stations. The symmetry would indicate the presence of nearly zero transequatorial wind at these hours. Correspondingly the vertical development of plasma bubbles is indicated in the sequence of ionograms over Campo Grande (mag. lat.:12º S) starting at 2250 UT on October 10 (**Fig. 9b)**. The oblique trace starting at 22:50 UT developing into spread F traces in successive ionograms is a clear indicator of bubble development, as the trace first appeared over CX at 22:10 UT (not shown here) followed by near simultaneous appearance, after a time delay of ~ 40 minute, over the two conjugate sites. This time delay (40 minutes) in the SF onsets over the conjugate sites, relative to that over the equator, points to a bubble vertical rise/development velocity of ~ 125 m/s (based on consideration of the conjugate point bottomside F layer at ~350 km being field line mapped to equatorial apex height of ~650 km). An exactly similar description holds for the spread F development sequence over the three stations on October 12 (also not shown here to save space) which was also marked by Vz variations identical to that of Oct.10. On the other hand, the Vz variation on October 23 (day 296) shows asymmetric patterns at the two conjugate stations, the peak amplitude of Vz (V_{zp}), at Campo Grande being 8 m/s larger than at Boa Vista. This might correspond to a northward (transequatorial) wind of ~ 25 m/s. The exact relationship between the ΔV_{zp} and TEW will be shown later. The F layer traces at Campo Grande for this evening, presented in the lower half of **Fig. 9b**, do not show any overhead spread F thereby suggesting total absence of any field aligned topside bubble development in the COPEX station meridian (even though the vertical drift of 75 m/s over the equator was well above the threshold limit for the bubble development, under very weak TEW, as discussed in Section 3.2.1). This sequence appears to provide direct evidence on the post

sunset ESF suppression by the transequatorial wind. It is a significant result from the COPEX campaign that is also supported by our recent findings on ESF suppression by meridional winds as obtained from digisonde data analysis, but using a different methodology (Abdu et al., 2006b).

3.5- Medium term trend in the transequatorial wind (TEW) and evening vertical drift

The evening vertical drift peak (Vzp) values at Cachimbo, obtained from the mean of the vertical drift variations calculated using two pairs of frequencies (4 & 5 MHz and 6 & 7 MHz), are plotted in **Fig. 10** (top panel) as a time series during the entire COPEX campaign period. It is to be noted that the Vzp values derived from the two frequency pairs are in general comparable to each other (with a few exceptions). The solar flux parameter F10.7 is plotted in the panel below. The difference between the V_{zp} values at the conjugate sites, V_{zp}(CG) - V_{zp}(BV), denoted as ΔV_{zp}(CG – BV) is plotted in the third panel. The difference between the conjugate point hmF2 values, as average of the 5-minute values in the 18-19 LT interval (indicated by shaded area of Fig. 7), denoted as ΔhmF2(CG – BV) is plotted in the bottom panel. We note large day-to-day variability in the Vzp, ΔVzp and ΔhmF2 values. Notwithstanding the same, the Vzp values show an increasing trend, as seen in the linear fit (panel 1), its average value increasing by ~10 m/s from early October to early December. Such an increase appears to be part of the seasonal variation in the Vzp whereby the December-January period has an annual peak in Vzp. Such an annual peak has been shown to be arising from the large westward magnetic declination angle that characterizes the Brazilian longitude sector (Abdu et al., 1981b). The Vzp is found to be strongly modulated by the F10.7, which brings out the well-known solar flux dependence of this parameter (Fejer et al., 1991). The large day-to-day variation in the Vzp during the interval from ~ day-300 to day-320 has been shown to be the result of a planetary wave episode (Abdu et al., 2006c). The difference between the vertical drifts at conjugate points, ΔV_{zp}(CG – BV), shows a steady increase towards December superposed on its day-to-day variability. The average values of ~ - 10 m/s in early October increased to 12 m/s in early December. This steady increase in ΔV_{zp}(CG – BV) indicates a corresponding increase of northward transequatorial wind consistent with the ΔhmF2 variation in the bottom panel as well as with the variation from October to December for 18-19 LT period seen in the plot in Fig. 8.

The relationship between the vertical drift and meridional wind at the conjugate stations can be expressed as follows. Besides the **E×B** vertical drift arising from a zonal electric field, a meridional wind causes vertical displacement of plasma due to finite magnetic field inclination, so that the net vertical drift υ_{eff} at a location with magnetic inclination I is the sum of the vertical drift due to the electric field, $\upsilon_z \cos(I)$, and that due to the magnetic meridional wind $U_{mm} \cos(I) \sin(I)$. Therefore the parameter ΔVzp can be expressed as:

$$\Delta Vzp_{(CG-BV)} = \upsilon_{eff\,(CG)} - \upsilon_{eff\,(BV)} = (U_{mmCG} + U_{mmBV}) \cos(I) \sin(I) \quad (1)$$

U_{mm} is considered positive northward in Eq.1. For the dip angle of the conjugate stations (23º) a change in $\Delta Vzp_{(CG-BV)}$ by 1 m/s corresponds to a change in the transequatorial wind by ~3 m/s. Thus we note (from the third lower panel of Fig 10) that the dVzp was -

10 m/s (as per the linear fit curve) during early October which corresponded a southward directed TEW of 30 m/s. The TEW became ~40 m/s northward during December (that represented an overall northward increase by 70 m/s). The average value of the coefficient $d(\Delta hmF2)/\Delta(U^N + U^S)$ during 18-19 LT, for which $\Delta hmF2_{(CG-BV)}$ parameter is plotted in Fig. 10, is close to 1.5, in units of km/(m/s) (see **Fig. 6**). The increase in the ΔhmF2 from October to December in **Fig. 10** is found to be ~90 km, which therefore corresponds to a change in the magnitude of TEW by ~60 m/s. (possible effect of such medium term variation in TEW on ESF will be briefly discussed in Section 4). Thus we note that the change in the TEW as obtained from the V_{ZP} measurement (70 m/s) is a bit higher than that inferred from the modeled hmF2 values (~60 m/s). Such a difference appears to be reasonable considering the rather rapid variation in the coefficient $d(\Delta hmF2)/\Delta(U^N + U^S)$ present around this local time (as per Fig. 6) and the height difference between hmF2 and the F layer bottomside heights at 4- 7 MHz plasma frequencies used for Vz calculation. Also, during the period (around the day 310) when ΔVzp is around zero the mean (best fit) ΔhmF2 does not become zero, presenting an offset by ~30 km. This situation seems to suggest the presence of certain hemispheric asymmetry between the COPEX stations arising from factors other than the TEW. A possible asymmetry of the neutral atmosphere, and the incident solar ionizing radiation, over the conjugate sites arising from the latitudinal separation between the geographic and dip equators (the geographic latitude of the BV and CG being 2.8°N and 20.5°S, respectively) can be a likely cause. A quantitative verification of this point is beyond the scope of this paper. We should point out, however, that in view of the offset just mentioned above, during the hours when Vz measurement by digisonde is reliable, particularly in the evening hours (near18-19 LT), the TEW appears to be better represented by ΔVzp than by ΔhmF2 values.

4. Discussion

The COPEX campaign results have brought to light some new findings/evidences on the post sunset spread F/plasma bubble irregularity development conditions and related issues as highlighted below. They range from the instability initiation characteristics, bubble development under the influences of the evening vertical drift (prereversal electric field enhancement), to the role of transequatorial/meridional winds on a day-to-day and medium term basis. The results also have provided new evidences on possible control (or lack of control) of the ESF development by changes in field line integrated conductivity represented by the variable presence of sporadic E layers at the feet of the unstable field lines, which is the subject of a separate paper by Batista et al. (2008). According to the theory of the Rayleigh-Taylor instability mechanism, believed to be responsible for the ESF/bubble development, an electron density perturbation needs to be initiated at the bottomside gradient region of a rising F layer for the instability to develop. The basic source of the initial perturbation, widely attributed to gravity wave flux originating from the lower atmosphere, is little understood and will not be discussed here any further. The linear growth rate for the instability process is dependent on the flux tube integrated quantities as explained by Haerendel et al. (1992). A generalized form of the linear growth rate as derived by Sultan (1996) is given by:

$$\gamma_{FT} = \frac{\Sigma_P^F}{\Sigma_P^E + \Sigma_P^F}\left(\frac{E}{B} - U_{FT}^P + \frac{g}{\nu_{eff}}\right)\frac{1}{L_{FT}} - \beta_{FT} \qquad (2)$$

Here $\sum_P^E$ and $\sum_P^F$ are the field line integrated conductivities for the E and F region segments of a field line; U_{FT}^P is the conductivity-weighted flux tube integrated vertical wind; β is the recombination loss rate; and ν_{eff} is the effective ion-neutral collision frequency. The subscript *FT* in Eq. 2 stands for flux tube integrated quantity. The influence of the different terms in the ESF variability has been discussed briefly in Sultan (1996) (see also, Abdu, 2001). Perhaps, the most observed effect on the ESF development is caused by the *E/B* term arising from the evening vertical drift enhancement (PRE) of which new results were presented above, and will be further discussed below. We note from Eq. 2, that a larger flux-tube integrated conductivity could reduce the instability linear growth rate. Even if γ_{FT} is sufficiently positive for the initiation of the instability the ensuing nonlinear growth of the instability developing into topside bubble structures can be retarded or even totally inhibited depending upon the magnitude of the flux-tube integrated conductivity which can be controlled by TEW/meridional winds as discussed by Maruyama (1988) and observationally verified by Abdu (1997) and Abdu et al. (2006b).

The ESF initiation process as detected from the appearance of the off-vertical echoes/satellite traces in the ionograms presented in **Fig. 2**, indicates the presence of wave disturbances as precursor to the SF traces in ionograms, as was discussed by Abdu et al. (1981a) from ionosonde observation over Fortaleza. The result presented here from the combined observations over the conjugate and dip equatorial sites of the precursor traces has important significance for elucidating the ESF onset processes. These traces appear to represent the large scale wave structure (LSWS) in the bottomside F region observed by the ALTAIR incoherent scatter radar that is identified as satellites traces in ionograms, as recently discussed by Tsunoda (2008). On the basis of the diagnostics by radar and digisonde pointing to similar feature as an ESF precursor signature we may call this off-vertical trace as LSWS trace or simply WS (Wave Structure) trace. The main F layer trace echoes are reflected close to vertical as verified from the second hop distance in the ionogram, and from digisonde sky maps. The wave structure traces just mentioned usually appear from the immediate west or east of the vertical in the majority of cases. Depending upon the observational cadence (5-minute in this case) the smallest detectable separation between the main trace and the closest WS trace can vary from less than 100 km to several hundred kilometers, compatible with the ~200 km east-west scale size for LSWS revealed in the steering mode incoherent scatter radar map of Tsunoda (2008) and the ray tracing results by Sales et al. (1996). The most important aspect of the present data is the simultaneous observation of the wave structure traces in the conjugate station ionograms, whereby a new insight into the dynamics of the trace evolution emerges **as described below**. In nearly all the cases examined in the COPEX campaign data set, the WS traces appear nearly simultaneously at the conjugate stations. But they are delayed by a few tens of minutes with respect to their appearance over the equatorial site. Such time delay is found to vary, from one day to another, from ~ 20 minutes to 45 minutes in the cases examined under quiet conditions. If the wave structure is the signature of electron density modulation by a propagating neutral wave disturbance (such as a gravity wave) then these results, (showing simultaneous occurrence at conjugate stations that is delayed with respect to the occurrence over the

equatorial station), would point (based on the COPEX station alignment shown in Fig.1b) to a magnetically westward propagating neutral disturbance front in the evening hours. While westward propagating gravity waves are expected to be present in the F layer bottomside (Fritts et al., 2008) that possibility appears unlikely to explain the present scenario given the well known day-to-day variability of the neutral wave dynamics. On the other hand we expect the plasma bubble development by the R-T instability mechanism to take place in unstable plasma flux tubes under conditions determined by the electric fields, conductivity and perpendicular and parallel currents of the entire flux tube (see, for example, Haerendel et al., 1992; Sultan, 1996; Keskinen et al., 2003), a situation that results in simultaneous instability growth along the entire flux tube which is manifested as vertical development of the depleted flux tubes above the equator. The corresponding latitudinal extension/expansion of the bubble "feet" could explain the near simultaneous appearances of the WS traces over the conjugate sites that are delayed by several minutes with respect to the first appearance of such traces over an equatorial site. A time delay of 30 minute for the WS appearance over the conjugate stations implies a bubble vertical rise velocity of ~ 120 m/s. This velocity is compatible with the available model and observational results (for example, Zalesak et al., 1982; Tsunoda, 1981; Abdu et al., 1983a). We note that the smaller scale structuring manifested in the diffuse echoes of the range spread trace, as part of the bubble, is already well developed at the equator by the time the WS trace marking the bubbles initiation first appears over the conjugate locations. The observed variable time delay on different days would indicate a correspondingly variable vertical rise velocity of plasma bubble structures developing over the equator. Thus the signatures of the LSWS/WS over the equatorial and conjugates sites, as described here, can be seen as direct manifestation of the vertical development of the flux tube aligned bubbles. Their continuing altitudinal/latitudinal development to topside bubbles structures are controlled by conditions set by the PRE, seed perturbation intensity, the transequatorial winds and the field line integrated conductivity. The present results in fact are evidence that the wave structure, manifested as off-vertical echoes, or satellite traces, in the post sunset equatorial ionograms, do indeed mark the onset of plasma bubble development. This evidence thus supports the view that the direct precursor to the ESF/plasma bubble development in the form of the LSWS seen by radar, as described by Tsunoda (2008), is the same as the off-vertical/satellites traces in ionogram simultaneously observed at conjugate sites as presented here as well as that reported earlier from single station observations (Abdu et al., 1981a).

The results in **Fig. 5** illustrate the control by Vz over the equator for different degrees of bubble development/rise velocity as manifested by the varying time delay in the spread F onset at off-equatorial latitudes. The larger evening vertical drift with peak value (Vzp) of around 60 m/s could result in rapid bubble rise velocity (>100 m/s) that caused post sunset spread F over Cachoeira Paulista at earlier post sunset local times (before 20 LT and 22 LT in the two cases considered). These cases can be classified as well-developed bubble events with the equatorial apex heights probably exceeding ~ 1000 km. Apparently the TEW that was present during these events, as indicated by a small degree of conjugate point asymmetry in the evening Vz (clearly seen in the Vzp values at BV and CG in **Fig. 5**, panels 1 and 2) did not have much influence on the bubble

growth in the presence of such large vertical drift. The case of the less developed bubbles with equatorial apex height not attaining the ~ 900 km height limit necessary for SF occurrence at Cachoeira Paulista corresponded to Vzp of only ~ 35 m/s (panel 3). The limit of Vzp for the case of the bubble growth not attaining an apex height of ~ 650 km, which is the limit for observing SF over the conjugate stations, is only ~ 30 m/s (panel 4). In other words, the Vzp should be > 30 m/s for the bubbles expand to 650 km that is the minimum height necessary for spread F to be observable over the conjugate stations. The lowest vertical drift of 22 m/s corresponded to the case of a stable post-sunset equatorial F region. Thus we have evidence of a systematic control by the evening vertical drift on the growth rate for the spread F/plasma bubble development. We note further that this systematic control is not likely affected by the TEW whose magnitude, it appears, was not expressive enough in the presence of the relatively larger V_{zp} values (Fig 5). These results are in reasonably good general agreement with the results from previous studies connecting Vzp with the ESF intensity (for example, Abdu et al., 1983b; Fejer et al., 1999) though these earlier studies did not consider the presence of the TEW. Thus, in the sense that a verification on the possible role of TEW was possible (although with little effect during the period analyzed), the COPEX data has permitted additional refinement in the relationship between the Vzp and ESF development. It should be pointed out here, that the picture described above is the results of a mean behavior. The connection between the changes in individual Vzp and ESF intensity is bound to present a good degree of variability on a day-to-day basis due to other factors such as the amplitude of a possible seeding source, the nature of the LSWS as observed here and as considered by Tsunoda (2008), the presence of a TEW of larger intensity, etc.

It is interesting to note in Fig 5 that the systematic decrease of the Vzp with the increasing delay for spread F onset at an off-equatorial latitude, (that is, with a decrease of the bubble rise velocity) is apparently associated with a systematic increase of the ∑Kp values. This might suggest that the post sunset decrease of the Vz could have a significant contribution from disturbance dynamo electric field that has westward polarity at these hours (see for example, Richmond et al., 2003). We may note further that the pre sunrise Vz, on the other hand, presents a systematic increase with the increase of the ∑Kp, again an indication of the presence of disturbance dynamo electric field which is eastward during this hours. Pre sunrise/post midnight increases in the F layer height and vertical drift near the equator occurring under quiet as well as disturbed conditions have been discussed before (Abdu et al., 1996; Nicolls et al., 2006). It is interesting to note that the intensity of the TEW (as reckoned from the difference of Vz between the conjugate stations, plotted in blue and red curves in Fig. 5) also increases during pre sunrise hours with increase of Kp. This might indicate the possibility of an asymmetric energy input for high latitude thermospheric heating that drives the equatorward winds, which has, under reduced plasma density (and hence reduced ion drag effect) of the pre sunrise hours, easier access to equatorial latitude. The corresponding signature on pre sunrise ESF development needs to be examined (however, see also, MacDougall et al., 1998). More detailed results on the disturbance features in the COPEX results will be the topic of a different paper.

The well developed large scale bubble structures in **Fig. 3** (as seen in the optical images) appear symmetrical over the conjugate stations, with their zonal drift velocities being exactly identical as well, as shown in the companion paper by Sobral et al. (2008). On the other hand, the smaller scale structures as observed in the ionograms present significant asymmetry. The background F layer characteristics over Boa Vista and Campo Grande were somewhat similar but not exactly identical. We note the foF2 values of 17 MHz and 16 MHz over BV and CG respectively which could indicate the presence of some degree of TEW directed northward at this time and hence possibly a corresponding asymmetry in the density gradient regions of the plasma bubble at conjugate locations. Results of 3-dimensional simulation of plasma bubble by Keskinen et al. (2003) showed larger density gradients inside a bubble when the ambient density is higher. Accordingly the different ambient densities at the conjugate sites verified in the ionograms of Fig. 3 could correspond to different degrees of density gradient within the bubbles and hence in the generation of secondary instabilities producing the medium scale structures (km or smaller scale sizes) detected with asymmetric echo intensities by the conjugate site digisondes. Also, the electric fields at such scale sizes do not field line map between the conjugate ionospheres (see, for example, Farley, 1960). This would lead us to conclude that the larger scale plasma bubble structures are symmetric with respect to the dip equator, while the smaller scales that cause radio wave scintillations and/or spread F traces in the ionograms may not show hemispheric symmetry, being influenced significantly by the local ionospheric conditions. In this context it is pertinent to recall that the L-band scintillation (measured by the GPS receivers) presented higher intensity over the conjugate sites as compared to the very weak intensity over the equator (Section 3.1). The background plasma density over the conjugate sites is higher than over the equator which could lead to density gradients in the instability development process that are more intense over the conjugate sites than over equator (as per the modeling results of Keskinen et al., 2003). Such a scenario should be an important cause of the observed scintillation intensity latitude distribution. This point deserves further investigation, however.

An important feature of the evening vertical drift enhancement (prereversal enhancement in the zonal electric field - PRE) revealed from the COPEX campaign results concerns the strong latitude/height gradient in this parameter. It appears to be more intense in the Brazilian longitude than that expected over Jicamarca for identical solar flux conditions. One of the driving factors of the PRE is known to be the thermospheric zonal wind (Rishbeth, 1971; Heelis et al., 1974; see also Batista et al., 1986) which is eastward in the evening and post-sunset hours. A latitudinal variation in the evening zonal wind should be able to produce a corresponding variation in the zonal electric field as well, as it appears to do in the vertical electric field (see for example, Anderson and Mendillo, 1983). If so, the rapid decrease of the vertical drift with increasing height/latitude might signify a correspondingly rapid latitudinal decrease in the zonal wind. This point needs to be verified from direct observations of the winds at these latitudes and from model simulation of PRE development based on such winds. The presence of a latitudinal gradient in the plasma bubbles zonal drift velocity suggesting a corresponding gradient in zonal winds in the Brazilian region has been reported by Sobral and Abdu (1990).

One of the interesting results from the COPEX campaign concerns the features of the TEW characterized by its large day-to-day variability (**Fig. 7**) as well as by its medium term trend of increasing northward intensity (**Fig. 10**). While the latter characteristics appear to originate from the solar declination angle variation during the campaign period, its possible influence on the seasonal variation of the ESF is of specific interest. The evening (18-19 LT) TEW varied from ~ 35 m/s southward in the beginning of October to as much northward in the beginning of December as per the ΔVzp parameter in Fig.10. During this period the spread F occurrence shows a systematic increase as part of its seasonal variation in the Brazilian longitude sector (Abdu et al., 1981b, Sobral et al., 2002) as shown in **Fig. 11** for Campo Grande. This SF seasonal trend does not clearly indicate a direct influence on its development from the TEW which should have manifested itself by a general increase of SF around the period of zero TEW. On the other hand we note that the Vzp variation over Cachimbo in **Fig. 10** (as seen in the linear fit curve) shows an increase by ~10 m/s during the same period. Based on the earlier discussion related to the results in **Fig. 5** we expect to see an increasing trend in SF occurrence/intensity as a result of an increasing trend in Vzp, which is indeed observed. Thus we note that the degree of medium term variation in TEW appears to be inadequate to dominate over the effect of a medium term variation in Vzp in controlling the ESF variation trend during this campaign period that covered only a limited part of spread F occurrence season over Brazil. This however, may not rule out any possible role of a larger intensity variation in TEW to explain the spread F seasonal variation as discussed, for example, by Maruyama and Matuura (1984).

Under unique conditions such as those represented in the results of **Fig. 9a** and **b** it appears possible to clearly identify the role of TEW in specific cases of ESF suppression. Here, on two of the three carefully selected evenings (October 10 and 12) the vertical drifts over Cachimbo are nearly the same as are the drifts over the two conjugate stations, which indicated near-zero TEW on these evenings. Consequently bubble development was initiated at 2250 UT (1910 LT) followed by continuing evolution of the SF traces in the subsequent ionograms. In contrast to this, on the third day (October 23), while the drift over Cachimbo is almost the same as on the other two days, that over the two conjugate stations differed significantly, which corresponded to a northward TEW of ~ 25 m/s. On this evening overhead bubble development did not take place over the COPEX stations, which revealed only some eastward drifting patches detected later on. Spread F was present over Cachimbo on this evening but apparently did not develop vertically to be observed at the conjugate sites. Thus in a case study like this it looks possible to verify the effect of TEW in suppressing/limiting the growth of top side bubble development. Similar case studies demonstrating the role of TEW in suppressing the ESF were made recently by Abdu et al. (2006b). In an earlier study (Abdu, 1997) it was pointed out that while the TEW is effective in suppressing the topside bubble development it appeared not as effective to suppress the F layer bottomside irregularities.

5. Conclusions

The results from the analysis of the COPEX campaign data presented here have brought out new insight into the dynamical and electro dynamical processes that control the post

sunset equatorial spread F development and evolution, besides providing new evidences in support of some of the already known aspects of the related coupling processes. The main conclusions of this study can be summarized as follows: (1)- Simultaneous measurements by Digisondes at the magnetic equator and conjugate locations have enabled the identification of large scale wave structures over the equator, that are precursor to spread F development, as indicating the initiation of the flux tube aligned plasma bubbles development over the equator. This is the first evidence that the wave structures (WS) manifested as off-vertical trace in the post sunset equatorial ionograms do indeed mark the initiation of plasma bubble development. The inferred bubble rise velocities are compatible with those determined from observations and model studies; (2) - While the larger scale plasma bubbles structures as seen in optical images are fairly symmetric with respect to the dip equator the smaller scales responsible for producing spread F traces in the ionograms (or radio wave scintillations) may not show hemispheric symmetry, being influenced significantly by the local ionospheric conditions. This is first time such evidence (though expected) is available from simultaneous diagnostics of the two irregularity domains; (3)- The evening prereversal enhancement in the vertical drift appears to exercise systematic control on the spread F/plasma bubble irregularity development during the COPEX period in such a way that increasing drift velocity is associated with increasing degree of vertical growth of the bubbles under the conditions of generally weak transequatorial winds; it also presents large day-to-day variability; (4). The evening vertical drift presents a large degree of negative gradient with height, which corresponds to a negative gradient with latitude as well, that is, the vertical plasma drift/zonal electric field decreases with increase of height and latitude. The degree of the gradient (in the decrease) appears to be more marked in the Brazilian longitudes than over Jicamarca for comparable solar flux conditions; (5) - The transequatorial winds were mostly northward during daytime and near midnight hours during the COPEX period. The daytime TEW appears to be significantly under-represented in the HWM93. There is large day-to-day variability in the TEW which is superimposed on a steady northward increasing trend associated with the progressive displacement from October to December of the sub-solar heating region to southern hemisphere; (6) - The magnitude of the TEW as obtained from the hemispheric asymmetry in Vzp appear to show general agreement (with some exceptions) with that obtained from the hemispheric asymmetry in hmF2 in the evening hours (around 18-19 LT), and the northward increase of TEW as part of the seasonal trend also shows general agreement between the two techniques; (7)- Nighttime foF2 increases in the hemisphere which is on the downwind side of the TEW; (8)- There is new evidence in the COPEX data based on case study that the ESF can be suppressed by enhancement (northward in this case) in the TEW; (9) The degree of medium term variation in TEW does not appear sufficient enough to dominate over the medium term variation in the Vzp in controlling the observed trend in the ESF occurrence/intensity during the campaign period. (10)- It appears that the magnitude of the TEW increases with increase in magnetic activity during pre sunrise hours in the present data. Analysis of the COPEX data is continuing.

Acknowledgements:

The authors wish to acknowledge the supports from FAPESP through the project 1999/00437-0, and CNPq through grants n^{o} 502804/2004-1, 500271/2003-8. BWR was supported by AF grant #FA8718-06-C-0072. Logistical support for the operations of the instruments at the conjugate sites (Campo Grande, Cachimbo and Boa Vista) was provided by the Brazilian Aeronautic Ministry's Instituto Tecnologico de Aeronautic (CTA) which is thankfully acknowledged.

List of Reference

Abdu, M. A. (1997) Major Phenomena of the Equatorial Ionosphere Thermosphere System under Disturbed Conditions, *J. Atmos. Sol. Terr. Phys.*, 59(13), 1505-1519.

Abdu, M. A. (2001), Outstanding problems in the equatorial ionosphere-thermosphere electrodynamics relevant to spread F, *J. Atmos. Sol. Terr. Phys.*,, 63, 869-884.

Abdu, M.A., J.A. Bittencourt, I. S. Batista (1981a), Some characteristics of spread F at magnetic equatorial station Fortaleza. *J. Geophys. Res.*, 86, 6836-6842.

Abdu, M.A., J.A. Bittencourt, I.S. Batista (1981b), Magnetic declination control of the equatorial F region dynamo field development and Spread-F, *J. Geophys. Res.*, 86, 11443-11446.

Abdu, M.A., R.T. Medeiros, J.H.A. Sobral, J. A. Bittencourt (1983a), Spread F plasma vertical rise velocities determined from spaced ionosonde observations, *J. Geophys. Res.*, 88, 9197-9204.

Abdu, M. A., R. T. Medeiros, J. A. Bittencourt, and I. S. Batista (1983b), Vertical ionization drift velocities and range spread F in the evening equatorial ionosphere, *J. Geophys. Res*., 88, 399-402.

Abdu, M.A., J.H.A. Sobral, P. Richards, M. M. De Gonzalez, Y.N. Huang, B.M. Reddy, Cheng, K., E. P. Szuszcewicz, I. S. Batista (1996), Zonal/Meridional wind and disturbance dynamo electric field control of the low-latitude ionosphere based on the SUNDIAL/ATLAS-1 Campaign, *J. Geophys. Res.*, 101(A12):26729-26740.

Abdu, M. A., I. S. Batista, H. Takahashi, J. MacDougall, J. H. A. Sobral, A. F. de Medeiros, and N. B. Trivedi (2003), Magnetospheric disturbance induced equatorial plasma bubble development and dynamics: A case study in Brazilian sector, *J. Geophys. Res.*, 108, A12, 1449, doi:10.1029/2002JA009721,

Abdu, M. A, I. S. Batista, B. W. Reinisch, J. R. de Souza., E. R. de Paula, J. H. A. Sobral, and T. W. Bullet (2004), Equatorial Spread F variability investigations in Brazil: Preliminary results from Conjugate Point Equatorial Experiments Campaign-COPEX, AGU spring meeting Montreal.

Abdu, M. A., I. S. Batista, B. W. Reinisch, J. H. A. Sobral, and A. J. Carrasco (2006a), Equatorial F region evening vertical drift during southern winter months: A comparison of observational data with IRI descriptions, *Adv. Space Res.*, 37, 1007-1017.

Abdu, M. A; K. N. Iyer, R. T. de Medeiros, I. S. Batista, and J. H A. Sobral (2006b), Thermospheric meridional wind control of equatorial spread F and evening prereversal electric field, *Geophys. Research Lett.*, 33, L07106, doi:10.1029/2005GL024835.

Abdu, M. A., P. P. Batista, I. S. Batista, C. G. M. Brum, A. Carrasco, and B. W. Reinisch. (2006c), Planetary wave oscillations in mesospheric winds, equatorial evening prereversal electric field and spread F, *Geophys. Res. Lett.*, 33, L07107, doi:10.1029/2005GL024837.

Abdu, M. A., E. A. Kherani, I. S. Batista, E. R. de Paula, and D. C. Fritts (2008), An evaluation of the ESF/bubble irregularity growth conditions under gravity wave influences based on observational data from the SpreadFEx campaign, SpreadFEx special issue, *Ann. Geophys*., submitted.

Anderson, D. N., and M. Mendillo (1983), Ionospheric conditions affecting the evolution of equatorial plasma depletions, *Geophys. Res. Lett.,* 10, 541-544.

Anderson, D. N., B. W. Reinisch, C. Valladares, J. Chau, and O. Veliz (2004), Forecasting the occurrence of ionospheric scintillation activity in the equatorial ionosphere on a day-to-day basis, *J. Atmos. Sol. Terr. Phys.,* 66, 1567- 1572.

Bailey, G. J., and N. Balan (1996), Low-latitude ionosphere-plasmasphere model, in Solar-Terrestrial Energy Program: Handbook of Ionospheric Models, edited by R. W. Schunk, Utah State Univ., Logan, Utah. pp. 173– 206.

Batista, I. S., M. A. Abdu, and J. A. Bittencourt (1986), Equatorial F-region vertical plasma drifts: Seasonal and Longitudinal Asymmetries in the American Sector, *J. Geophys. Res.*, 91, 12055-12064.

Batista, I. S., M. A. Abdu, A. J., Carrasco, B. W. Reinisch, E. R.de Paula, N. J. Schuch, and F. Bertoni (2008), Equatorial spread F and sporadic E-layer connections during the Brazilian Conjugate Point Equatorial Experiment –COPEX, *J. Atmos. Sol. Terr. Phys.*, 70, 1133-1143.

Bertoni, F., I. S. Batista, M. A. Abdu B. W. Reinisch, and E. A. Kherani (2006), A comparison of ionospheric vertical drift velocities measured by digisonde and incoherent scatter radar at the magnetic equator, *J. Atmos. Sol. Terr. Phys.*. 68 (16): 1851-1852.

Bittencourt J. A., and Y. Sahai (1978), F-region neutral winds from ionosonde measurements of hmF2 at low latitude magnetic conjugate regions, *J. Atmos. Terr. Phys.,* 40(6), 669-676.

Bittencourt, J.A. and M. A. Abdu (1981), A Theoretical Comparison Between Apparent and Real Vertical Ionization Drift Velocities in the Equatorial F-Region, *J. Geophys. Res.*, 86, 2451-2455.

Burke, W. J., C. Y. Huang, L. C. Gentile, and I. and Bauer (2004), Seasonal-Longitudinal variability of equatorial plasma bubbles, *Ann. Geophys.*, 22, 3089-3098.

Casagrove, R. and R. T. Tsunoda (2002), A direction dependent instability of sporadic E layer in the nighttime mid-latitude ionosphere, *Geophys. Res. Lett.*, 29(18), 1864, doi: 10.1029/2002GL014669.

Devasia, C. V., N. Jyoti, K. S. Viswanathan et al. (2002), On the possible linkage of thermospheric meridional winds with equatorial spread F, *J. Atmos. Sol. Terr. Phys.*, 64, 1- 12.

Farley, D. T. (1960), A. theory of electrostatic fields in the ionosphere at non polar geomagnetic latitude, *J. Geophys. Res.*, 65 (3): 869-877.

Farley, D. T., B. B. Balsley, R. F. Woodman (1970), Equatorial spread F –Implications of VHF radar observations, *J. Geophys. Res.*, 75 (34), 7199.

Fejer, B. G., E. R. de Paula, S. A. Gonzalez, and R. F. Woodman (1991), Average vertical and zonal F-region plasma drifts over Jicamarca, *J. Geophys. Res., 96*, 13,901–13,906.

Fejer, B. G., L. Scherliess, and E. R. de Paula (1999), Effects of the vertical plasma drift velocity on the generation and evolution of equatorial spread *F*, *J. Geophys. Res.*, *104*, 19,859–19,870.

Fritts D. C., S. L Vadas, D. M. Riggin, M. A. Abdu, I. S. Batista, H. Takahashi, A. Medeiros, F. Kamalabadi, H.-L. Liu, B. G. Fejer, and M. J. Taylor, Gravity wave and tidal influences on equatorial spread F based on observations during the Spread F Experiment (SpreadFEx), *Ann. Geophys.*, in press, 2008.

Haerendel, G., J. V. Eccles, and S. Cakir (1992) Theory for modeling the equatorial evening ionosphere and the origin of the horizontal plasma flow, *J. Geophys. Res.*, 97 (A2), 1209-1223.

Hanson, W. B., S. Sanatani (1973), Large Ni gradients below the equatorial F peak, *J. Geophys. Res., 78,* 1167- 1173.

Hedin, A. E., E. L. Fleming, A. H. Manson, F. J. Schmidlin, S. K. Avery, R. R. Clark, S. J. Franke, G. J. Fraser, T. Tsuda, F. Vial, and R. A. Vincent (1996), Empirical wind model for the upper, middle and lower atmosphere, *J. Atmos. Sol. Terr. Phys.,* 58, 1421-1447.

Heelis, R. A., P. C. Kendall, R. J. Moffet, D. W. Windle, and H. Rishbeth (1974), Electrical coupling of the E- and F- region and its effects on the F-region drifts and winds, *Planet. Space Sci.*, *22*, 743–756.

Hysell, D. L., and E. Kudeki, E. (2004), Collisional shear instability in the equatorial F region ionosphere, *J. Geophys. Res.*, 109, A11301, doi: 10.1029/2004JA010636.

Jyoti N., C. V. Devasia, R. Sridharan, and D. Tiwari (2004), Threshold height $(h'F)_c$ for the meridional wind to play a deterministic role in the bottomside spread F and its dependence on solar activity, *Geophys. Res. Lett.,* 31, L12809, doi:10.1029/2004GL019455.

Kelley, M. C. (1989), The Earth's ionosphere, plasma Physics and Electrodynamics, Academic Press, San Diego, Calif.

Keskinen, M. J., S. L. Ossakow, and B. G. Fejer (2003). Three-dimensional nonlinear evolution of equatorial ionospheric spread-F bubbles, *Geophys. Res. Lett.*, 30(16), 1855, doi: 10.1029/2003GL017418.

Kil, H., and R. A. Heelis (1998), Global distribution of density irregularities in the equatorial ionosphere, *J. Geophys. Res.*, 103, 407-417.

Khmyrov, G. M., I. A. Galkin, A. V. Kozlov, B. W. Reinisch, J. McElroy, and C. Dozois (2008), Exploring digisonde ionogram data with SAO-X and DIDBase, in *Radio Sounding and Plasma Physics, AIP Conf. Proc. 974*, 175-185.

Kozlov, A. and V. V. Paznukhov (2008), Digisonde drift analysis software, in *Radio Sounding and Plasma Physics, AIP Conf. Proc. 974*, 167-174.

Kudeki, E., A. Akgiray, M. Milla, J. L. Chau, and D. L. Hysell (2007), Equatorial spread-F initiation: post-sunset vortex, thermospheric winds, gravity waves, *J. Atmos. Sol. Terr. Phys.*, 69, 2416-2427.

MacDougall, J.W., M. A. Abdu, P.T. Jayachandran, J.F. Cecile, and I.S. Batista (1998), Pre-sunrise spread-F at Fortaleza, *J. Geophys. Res.*, 103(A10):23415-23425.

Maruyama, T. (1988), A diagnostic model for equatorial spread F, 1, Model description and application to electric fields and neutral wind effects, *J. Geophys. Res.*, 93, 14611-14622.

Maruyama, T., and N. Matuura (1984), Longitudinal variability of annual changes in activity of equatorial spread F and plasma bubbles, *J. Geophys. Res.*, 89, 10903.

Maruyama, T., M. Kawamura, S. Saito, Nozaki, K Kato, H. Hemmakorn, N. Boonchuk, T. Komolmis, and Ha. Duyen (2007), Low latitude ionosphere-thermosphere dynamics studies with ionosonde chain in Southeast Asia, *Ann. Geophys.*, 25, 1569-1577.

McNamara, L. F., J. Retterer, M Abdu, M. A., I. S. Batista, and B. W. Reinisch (2008), F2 Peak Parameters, Drifts and Spread F derived from Digisonde Ionograms for the COPEX Campaign in Brazil, *J. Atmos. Sol. Terr. Phys.,* 70, 1144-1158.

Medeiros, R.T., M. A. Abdu, and I. S. Batista (1997), Thermospheric meridional wind at low latitude from measurement of F-layer peak height, *J. Geophys. Res.*, 102(A7):14531-14540.

Mendillo, M., J. Meriwether, and M. Biondi (2001), Testing the thermospheric neutral wind suppression mechanism for day-to-day variability of equatorial spread *F*, *J. Geophys. Res.*, *106*(A3), 3655–3663.

Muella T. A. H., E. R. de Paula, I. J. Kantor, I. S. Batista , J. H. A. Sobral , M. A. Abdu, K. M. Groves, P. M. Kintner, and P. F. Smorigo **(**2008), GPS L-Band Scintillations and Ionospheric Irregularity Zonal Drifts Inferred at Equatorial and Low Latitude Regions, *J. Atmos. Sol. Terr. Phys.*, 70, 1261-1272..

Nicolls, M. J., M. C. Kelley, M. N. Vlasov, Y. Sahai, P.R. Fagundes, F. Becker-Guedes, and W. L. C. Lima (2006), Observation and modeling of post-midnight uplifts near the magnetic equator, *Ann. Geophys.*, 24, 1317- 1331.

Otsuka, Y., K. Shiokawa, and T. Ogawa (2002), Geomagnetic conjugate observations of equatorial airglow depletions, *Geophy. Res. Lett., 29(15),* 1753, doi: 10.1029/2002GL015347.

Pingree, J. E., and B. G. Fejer (1987), On the height variation of the equatorial F region vertical plasma drifts, *J. Geophys. Res., 92,* 4163– 4166.

Prakash, S. (1999), Production of electric field perturbations by gravity wave winds in the E region suitable for initiating equatorial spread F, *J. Geophys. Res*., 104, A5, 10,051-10,069.

Raghavarao, M., Nageswara Rao, J. H. Sastri, G. D. Vyas, and M. Srirama Rao (1988), Role of equatorial ionization anomaly in the initiation of equatorial spread F, *J. Geophys. Res.*, 93, 5959-5964.

Rastogi, R. G. (1980), Seasonal and solar cycle variation of equatorial spread F in the American zone, *J. Atmos. Terr. Physics*, 47,593-597.

Reinisch, B. W. (1996). Modern Ionosondes, in *Modern Ionospheric Science*, edited by H. Kohl, R. Rüster, and K. Schlegel, European Geophysical Society, 37191 Katlenburg-Lindau, Germany, pp. 440-458.

Reinisch, B. W., M. A. Abdu, I. S. Batista, G. S. Sales, G. Khmyrov, T. A. Bullet, J. Chau, and V. Rios (2004), Multistation digisonde observations of equatorial spread F in South America, *Ann. Geophys.*, 22, 3145-3153.

Richmond A. D, C. Peymirat, and R. G. Roble (2003), Long-lasting disturbances in the equatorial ionospheric electric field simulated with a coupled magnetosphere-ionosphere-thermosphere model , *J. Geophys. Res., 108* (A3): Art. No. 1118 MAR 14.

Rishbeth, H. (1971), Polarization fields produced by winds in the equatorial F region, *Planet. Space Sci.*, *19*, 357–369.

Rishbeth, H., S. Ganguly, and J. C. G. Walker (1978), Field- aligned and field-perpendicular velocities in the ionospheric F2 layer, *J. Atmos. Terr. Phys*., 40, 767-784.

Saito, S., and T. Maruyama (2006), Ionospheric height variations observed by ionosondes along magnetic meridian and plasma bubble onsets, *Ann. Geophys.* 24, 2991-2996.

Sales, G., B. Reinisch, J. Scali, C. Dozois, T. Bullett, E. Weber, and P. Ning (1996), Spread F and the structure of equatorial ionization depletions in the southern anomaly region, *J. Geophys. Res*., 101(A12), 26819-26827.

Sastri, J. H., M. A. Abdu, I. S. Batista. and J. H. A. Sobral (1997), Onset Conditions Of Equatorial (Range) Spread-F At Fortaleza, Brazil, During The June Solstice, *J. Geophys. Res., 102(A11),* 24013-24021.

Scali, J. L., B. W. Reinisch, C. J. Heinselman, and T. Bullett (1995), Coordinated digisonde and incoherent scatter radar F region drift measurements at Sondre Stromfjord, *Radio Sci., 30*, 1481-1498.

Scherliess, L., and B. G. Fejer (1999), Radar and satellite global equatorial F region global equatorial F region vertical drift model, *J. Geophys. Res.*, 104, 6829-6842.

Sekar, R. and R. Raghavarao (1995) Critical role of the equatorial topside F region on the evolutionary characteristics of the plasma bubbles, *Geophys. Res. Lett.*, 22, 23, 3255-3258.

Sobral, J. H. A., and M. A. Abdu (1990) Latitudinal gradient in the plasma bubble zonal velocities as observed by scanning 630mm airglow measurements, *J. Geophys. Res., 95(A6),* 8253-8257.

Sobral, J. H. A, M. A. Abdu, T. R. Pedersen, V. M. Castilho, D.C. S. Arruda, M. T. A. H. Muella, I. S. Batista, M. Mascarenhas, E. R. de Paula, P. M. Kintner, A. E. Kherani, A. F. Medeiros, R. A> Buriti, H. Takahashi, N. J. Schuch, C. M. Denardini, C. J. Zamlutti, A. Pimenta, J. R. de Souza, F. C. Bertoni (2008), Ionospheric zonal velocities at conjugate points over South America: Experimental observations and theoretical validations during the COPEX campaign, this issue.

Sobral, J. H. A., M. A. Abdu, H. Takahashi, M. J. Taylor, E. R. de Paula, C. J. Zamlutti, and G. L. Borba (2002), A Study of the Ionospheric Plasma Bubbles Climatology over *Brazil, based on 22 years (1977-1998) of OI 630nm airglow Observation, J*. Atmos. Solar-Terr. Phys., 64, 12-14, 1517-1524.

Souza, J. R., M. A. Abdu, I. S. Batista, and G. J. Bailey (2000), Determination of vertical plasma drift and meridional wind using the Sheffield University Plasmasphere Ionosphere Model and ionospheric data at equatorial and low latitudes in Brazil: Summer solar minimum and maximum conditions, *J. Geophys. Res*., 105 (A6), 12813-12821.

Sridharan, R., D. Pallam Raju, R. Raghavarao, and P. S. V. Rao, Precursor to equatorial spread F in the OI 630 nm dayglow, *Geophys. Res. Lett*., 21, 2797- 2800, 1994.

Su S. –Y., C. K. Chau, and C. H. Liu (2008), On monthly/seasonal/longitudinal variation of equatorial irregularity occurrences and their relationship with the postsunset vertical drift velocities, *J. Geophys. Res.*, 113, A05307, doi:10.1029/2007JA012809.

Sultan, P. J. (1996), Linear theory and modeling of the Rayleigh_Taylor instability leading to the occurrence of equatorial spread F, *J. of Geophys. Res*., 101, 26875-26891.

Thampi Smitha V., Sudha Ravindran, Tarun Kumar Pant, C. V. Devasia, P. Sreelatha, and R. Sridharan (2006), Deterministic prediction of post-sunset ESF based on the strength and asymmetry of EIA from ground based TEC measurements: Preliminary results, *J. Geophys. Res*., 33, L13103, doi:10.1029/2006GL026376.

Tsunoda R. T. (1981), Time evolution and dynamics of equatorial back-scatter plumes, 1 Growth phase, *J. Geophys. Res.*, 86, 139.

Tsunoda, R. T. (1985), Control of the seasonal and longitudinal occurrence of equatorial scintillation by the longitudinal gradient in the integrated E region conductivity, *J. Geophys. Res.*, 90, 447-456.

Tsunoda, R. T. (2007). Seeding of equatorial plasma bubbles with electric fields from and Es-layer instability, *J. Geophys. Res.*, 112, A06304, doi: 10.1029/2006JA012103.

Tsunoda, R. T. (2008), Satellite traces: An ionogram signature for large-scale wave structure and a precursor for equatorial spread F, *Geophys. Res., Lett*., 35, L20110, doi:10.1029/2008GL035706.

Valladares, C. E., S. Basu, K. Groves, M. P. Hagan, D. Hysell, A. J. Mazella Jr., and R. E. Sheehan (2001), Measurement of the latitudinal distributions of total electron content during equatorial spread *F* events, *J. Geophys. Res.*, *106*, 29,133–29,152.

Woodman, R. F., and C. LaHoz (1976), Radar observations of F region equatorial irregularities, *J. Geophys. Res., 81*, 5447-5466.

Zalesak, S. T., S. L. Ossakow, and P. K. Chaturvedi (1982), Nonlinear equatorial spread F: The effect of neutral winds and background Pedersen conductivity, *J. Geophys. Res.,* **87**, 151.

Figure Captions:

Fig. 1a: A schematic of the COPEX geometry showing the magnetic field line connection between the conjugate E layers and the equatorial F layer peak/bottomside.

Fig. 1b: COPEX campaign station sites, Boa Vista - northern conjugate point, Campo Grande – southern conjugate point, and Cachimbo close to the magnetic equator. Also included are the locations of the permanent ionosonde stations in Brazil, Sao Luis, Fortaleza and Cachoeira Paulista, and Jicamarca in Peru.

Fig. 2: Sequential ionograms over Boa Vista (left), Cachimbo (middle) and Campo Grande (right). The arrows pointed at the F layer traces at each station shows the first appearance of an off- vertical trace close to the main F trace indicative of the start of a large scale "wave structure" as a precursor to the range spreading. The time delay between the first appearance of the "wave structure" at Cachimbo (at 22:05 UT) and that at the two conjugate stations (at 22:45 UT) indicates the vertical rise velocity (growth rate) of a flux tube aligned bubble developing over equator. (The additional traces that appear prior to 22:45 over Boa Vista are caused by multiple reflections between the sporadic E layer and the F layer).

Fig. 3: Illustrative ionograms over Boa Vista and Campo Grande and the simultaneous all-sky images on the night of October 09, 2002.

Fig. 4: Vertical drift velocities versus UT over the three COPEX sites mass plotted for entire campaign period.

Fig. 5 Mean vertical drift velocities over the three COPEX sites are plotted for different groups of days: Panel (1) - for the cases of early spread F occurrence (at or before 20 LT) over Cachoeira Paulista; Panel (2) - for the group of days when SF occurred at and before 22 LT over CP; Panel (3)- for the group of days when SF did not occur before midnight over Cachoeira Paulista; and Panel (4) - for the group of days when SF did not occur over Campo Grande and CP. (ΣKp: the daily sum of the 3-hourly Kp values representing the mean value for the days considered). Station names are BV; Boa Vista; CX: Cachimbo; and CG: Campo Grande. In the x-axis the LT exceeding 24 hours corresponds to a new day so that 24 should be subtracted from those values.

Fig. 6: Lower panel shows the SUPIM simulation results on the difference in hmF2 between the two conjugate stations, $\Delta hmF2_{(CG-BV)}$, obtained by subtracting the hmF2 simulated over Boa Vista from that over Campo Grande and the corresponding Transequatorial Wind, TEW (sum of the meridional winds at the two conjugate locations according to the HWM93.; the top panel shows the corresponding ratio of $d(\Delta hmF2)/\Delta(U^N + U^S)$.

Fig. 7: The lower panel shows a mass plot of the parameter $\Delta hmF2_{(CG-BV)}$ observed on all days of the COPEX campaign; in the upper panel the green curve shows the mean values with standard deviation of the mass plot, the blue curve represents the $\Delta hmF2_{(CG-BV)}$ modeled by the SUPIM using the meridional wind input as per the HWM93, and the orange curve shows the corresponding transequatorial wind (TEW).

Fig. 8: The $\Delta hmF2_{(CG-BV)}$ parameter for 4 quiet days of October and 6 quiet days of December, 2002, (left panels) and the corresponding $\Delta foF2_{(CG-BV)}$ variations (right panel). The results for October (December) are in the upper (lower) panels.

Fig. 9a: Vertical drift velocities over Cachimbo (left panel), Boa Vista (middle panel) and Campo Grande (right panel), during three quiet days October 10, 12 and 23 when they were nearly equal on all the three days during sunset time over Cachimbo, on two days (October 10 and 12) they were comparable/symmetric, while on one day (October 23) they were asymmetric, over the conjugate stations.

Fig. 9b: The set of 9 panels in the upper half of the figure shows ionograms at 5-minute interval from, 22:35 UT (~19:00 LT) till 23:15 UT (~19:40 LT) on October 10, 2002. Development of rather intense spread F can be seen being initiated from the `off-vertical trace` in the 22:50 UT (19:10 LT) ionogram. Well developed spread F traces continued past the last ionogram presented here. The lower set of nine panels shows ionograms similar to above starting at 23:10 UT (19:30 LT) for October 23, 2002. Here no overhead spread F development is noted.

Fig. 10: The peak amplitude of the evening vertical drift (Vz) enhancement, Vzp, plotted for the entire COPEX Campaign period in the top panel. Solar flux index F10.7 (second panel from top); The difference in the Vzp values at the conjugate stations by subtracting the Vzp over Boa Vista from that of Campo Grande denoted as $dVzp_{(CG-BV)}$ is in the third panel; and the corresponding difference in the hmF2 values denoted as $dhmF2_{(CG-BV)}$ is in the bottom panel. The data gap around the day 310 is due to the fact that the BV digisonde did not operate during this period.

Fig. 11: Ionogram spread F intensity, indexed as `1` (spread range < 100 km marked yellow), `2` (100 km < spread range < 200 km marked orange), and `3` (200 km < range spreading < 300 km marked brown), and darker shading for spread range > 300 km, as a function of UT and the day of year during the COPEX campaign period.

Table -1

	CACHIMBO	BOA VISTA	C. GRANDE	SÃO LUÍS	C. PAULISTA
LATITUDE	9.5S	2.8N	20.5S	2.6S	22.7S
LONGITUDE	54.8W	60.7W	54.7W	44.7W	45W
DIP ANGLE	-4.2	22.0	-22.3	-3.85	-33.7
MAG.LATITUDE	-2	11	-11	-1.6	-16
DECLINATION	-16.7	-14	-15.1	-20.7	-20.6

Table -2

BOA VISTA:	Digisonde DPS4; All Sky imager; GPS scintillation monitor(2); GPS TEC monitor; VHF receivers; Magnetometer
CACHIMBO & ALTA FLORESTA:	Digisonde DPS4; GPS scintillation monitor (2); GPS TEC monitor; VHF receivers; 30 MHz Radar
CAMPO GRANDE:	Digisonde DPS4; All Sky imager; GPS scintillation monitor (2); GPS TEC monitor; VHF receivers; Magnetometer
SÃO LUÍS::	Digisonde DGS256; GPS scintillation monitor; Magnetometer
C. PAULISTA:	Digisonde DGS256; GPS scintillation monitor

11PM -12 Sept 2008

Figures:

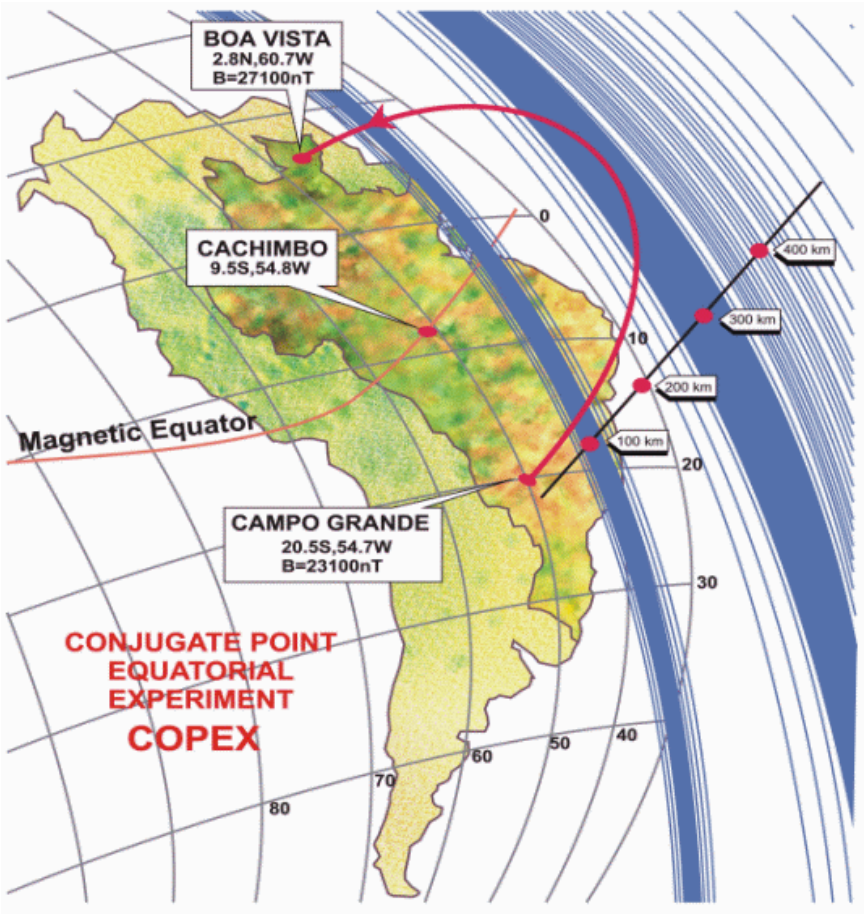

Fig. 1

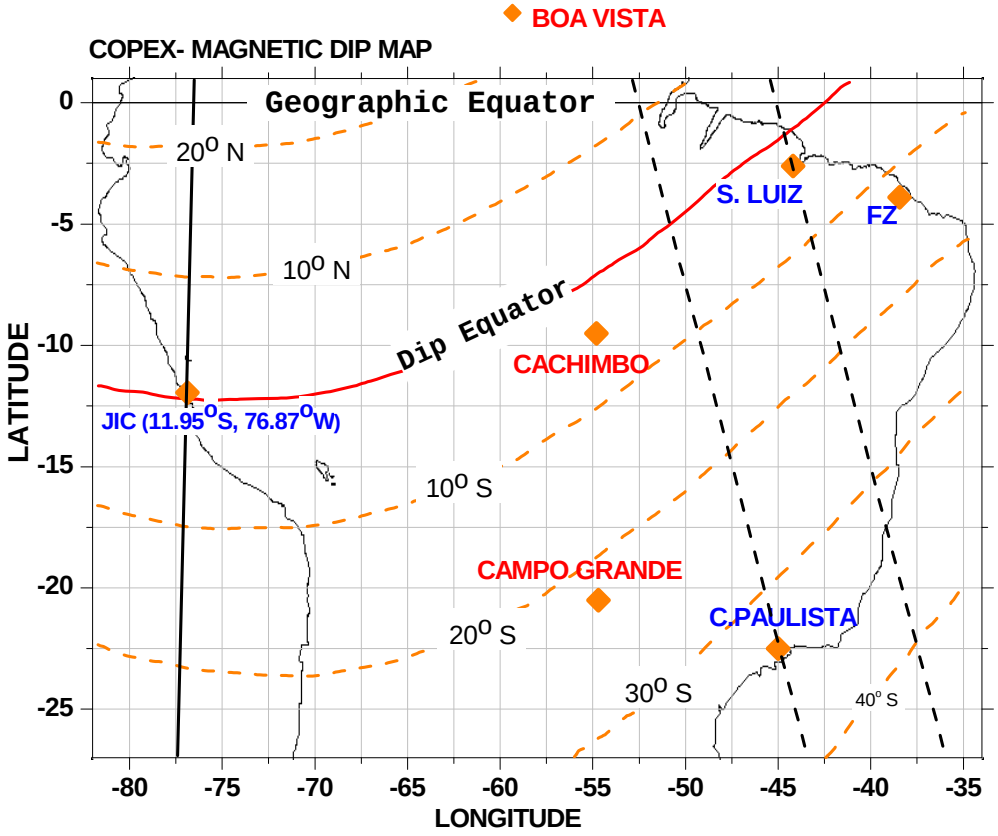
BOA VISTA
COPEX- MAGNETIC DIP MAP
Geographic Equator
20° N
10° N
Dip Equator
S. LUIZ
FZ
CACHIMBO
JIC (11.95°S, 76.87°W)
10° S
CAMPO GRANDE
C.PAULISTA
20° S
30° S
40° S
LATITUDE
LONGITUDE
0
-5
-10
-15
-20
-25
-80
-75
-70
-65
-60
-55
-50
-45
-40
-35

Fig. 1b

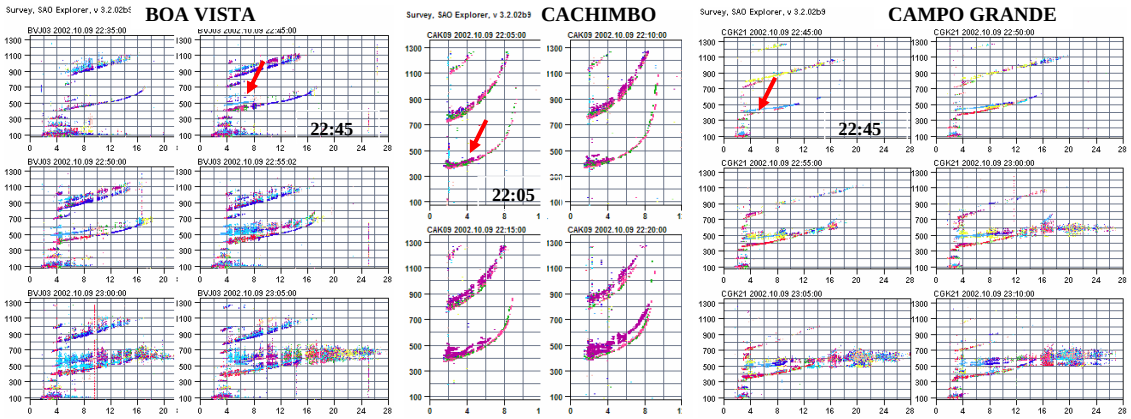

OCTOBER 09, 2002
Fig. 2

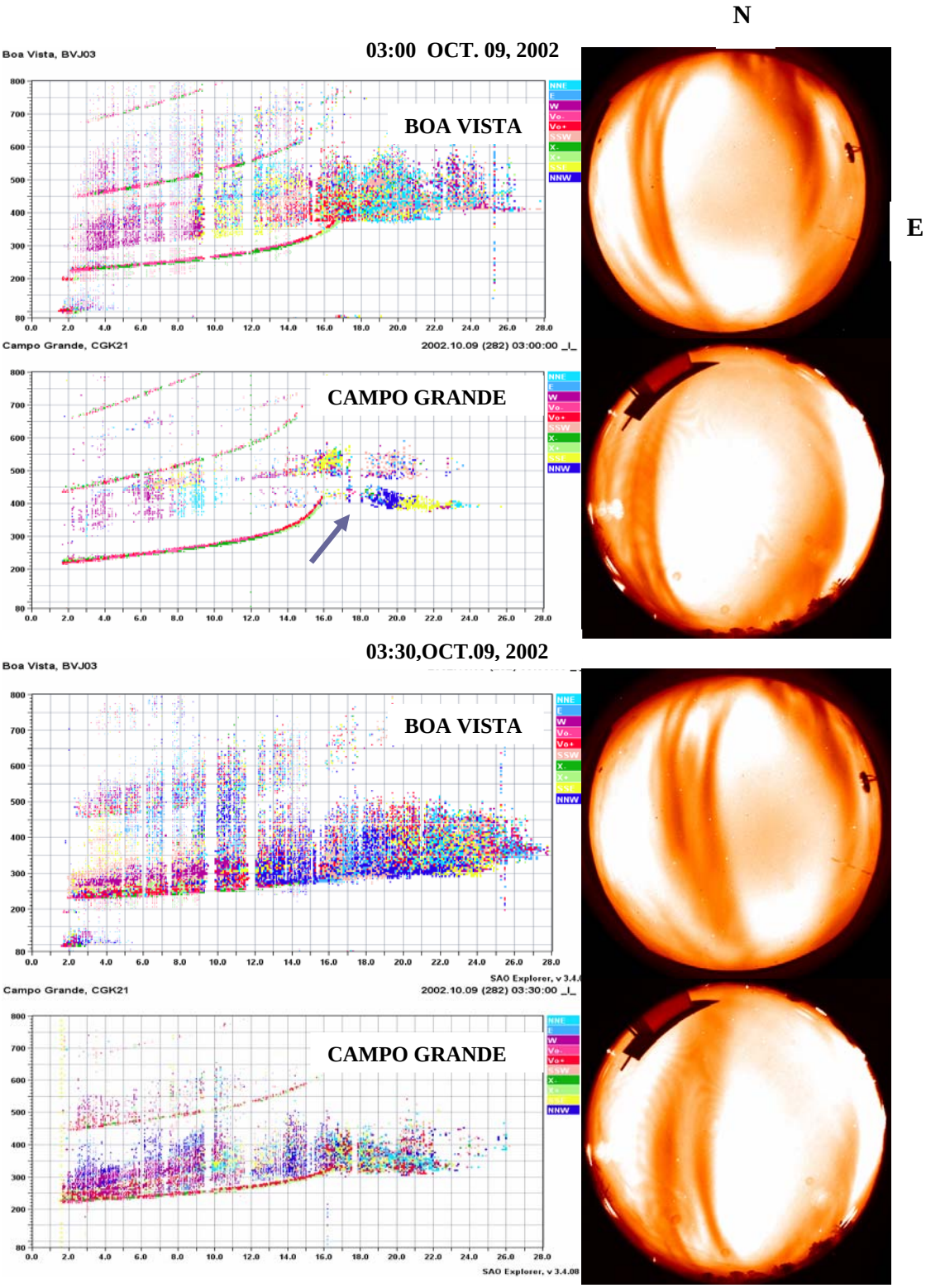
N
E
03:00 OCT. 09, 2002
Boa Vista, BVJ03
BOA VISTA
Campo Grande, CGK21
2002.10.09 (282) 03:00:00
CAMPO GRANDE
03:30,OCT.09, 2002
Boa Vista, BVJ03
BOA VISTA
Campo Grande, CGK21
2002.10.09 (282) 03:30:00
CAMPO GRANDE

Fig. 3

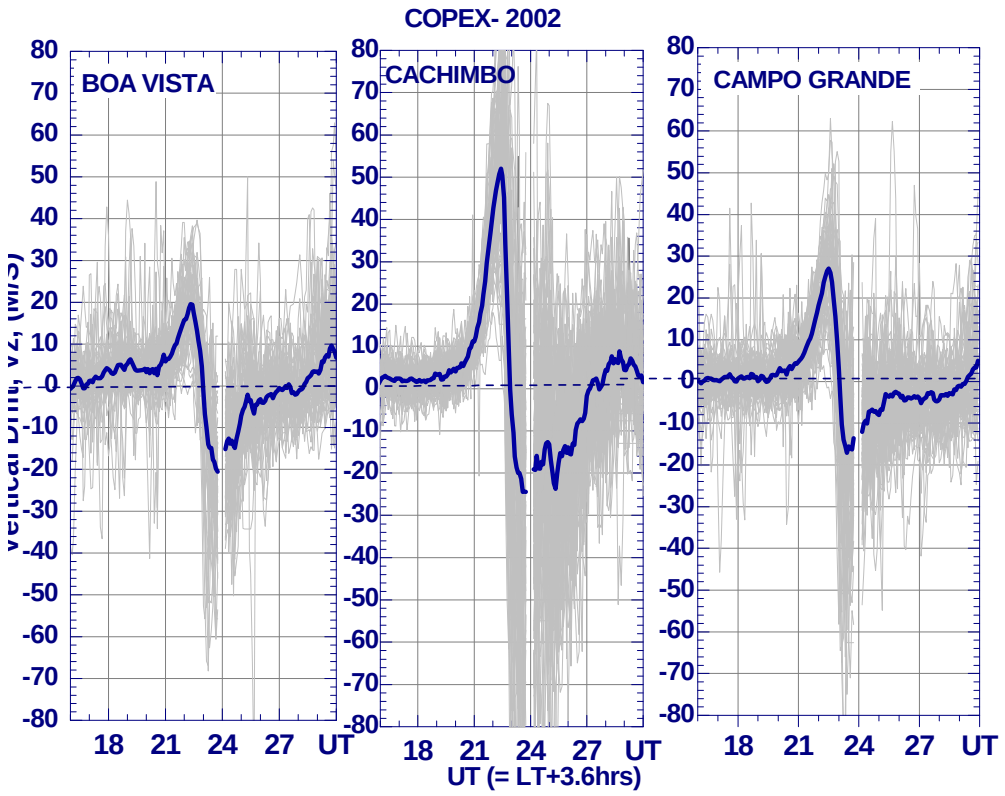

Fig. 4

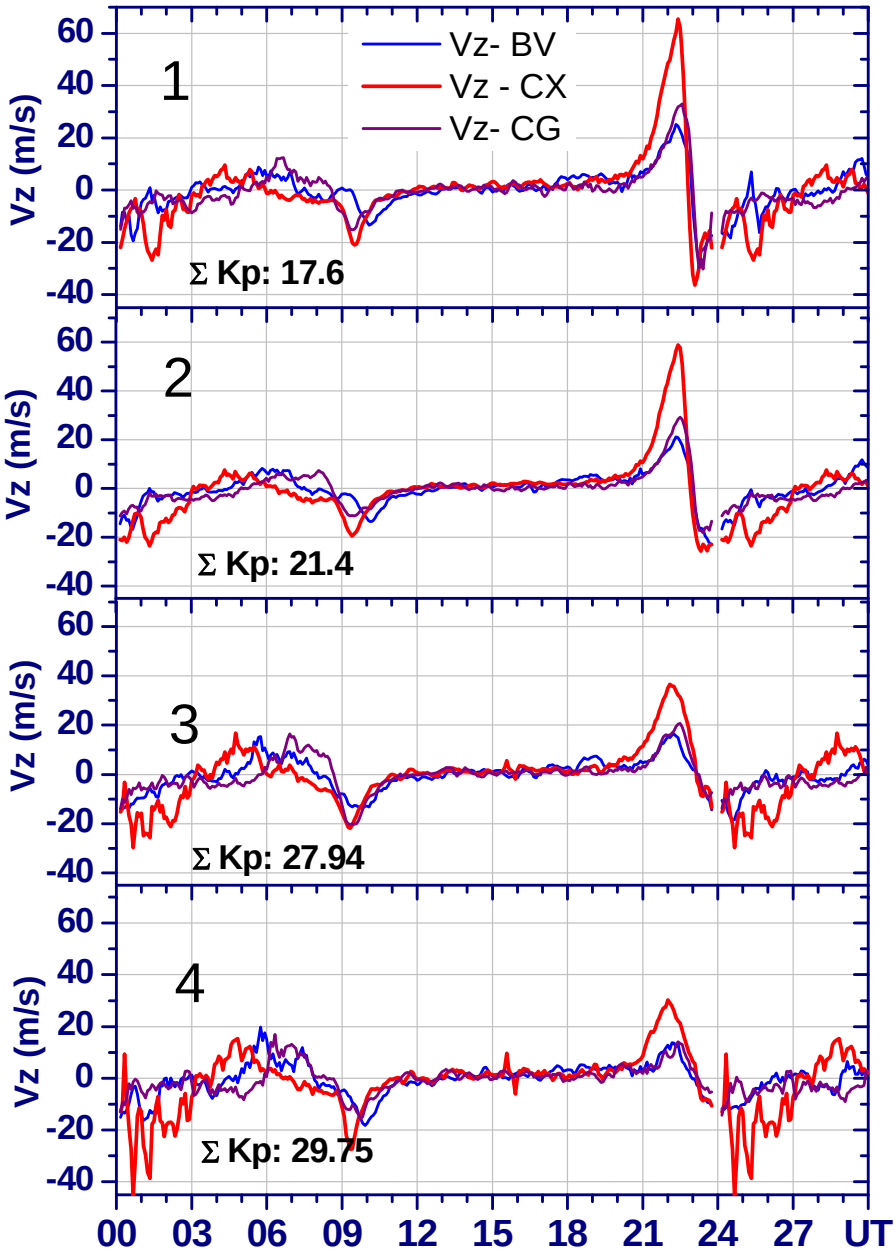
1
2
3
4
Vz- BV
Vz - CX
Vz- CG
Σ Kp: 17.6
Σ Kp: 21.4
Σ Kp: 27.94
Σ Kp: 29.75
Vz (m/s)
60
40
20
0
-20
-40
00
03
06
09
12
15
18
21
24
27
UT

Fig. 5

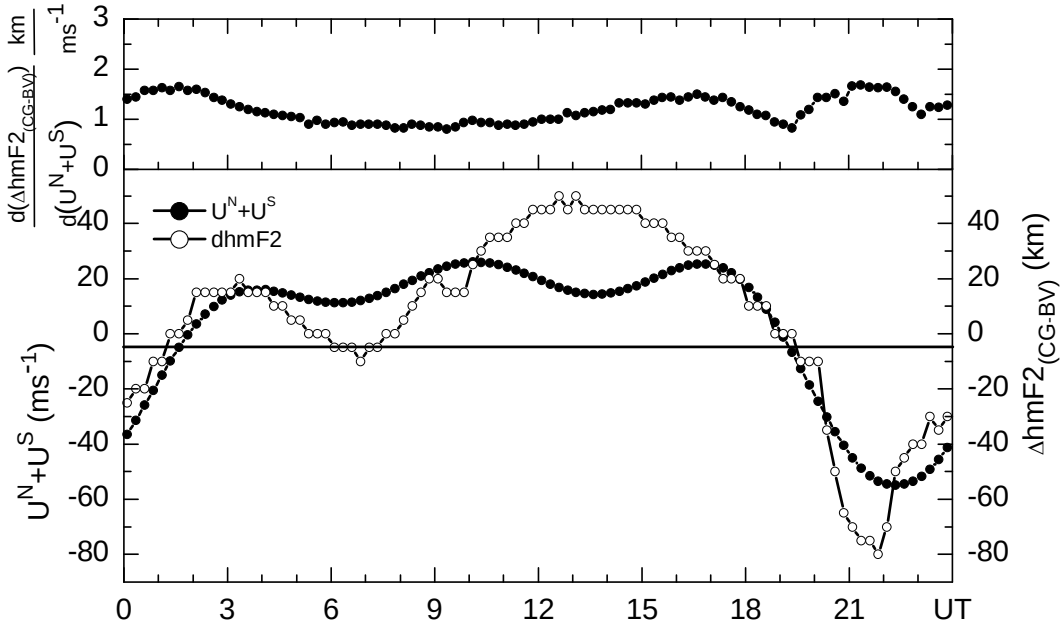

Fig. 6

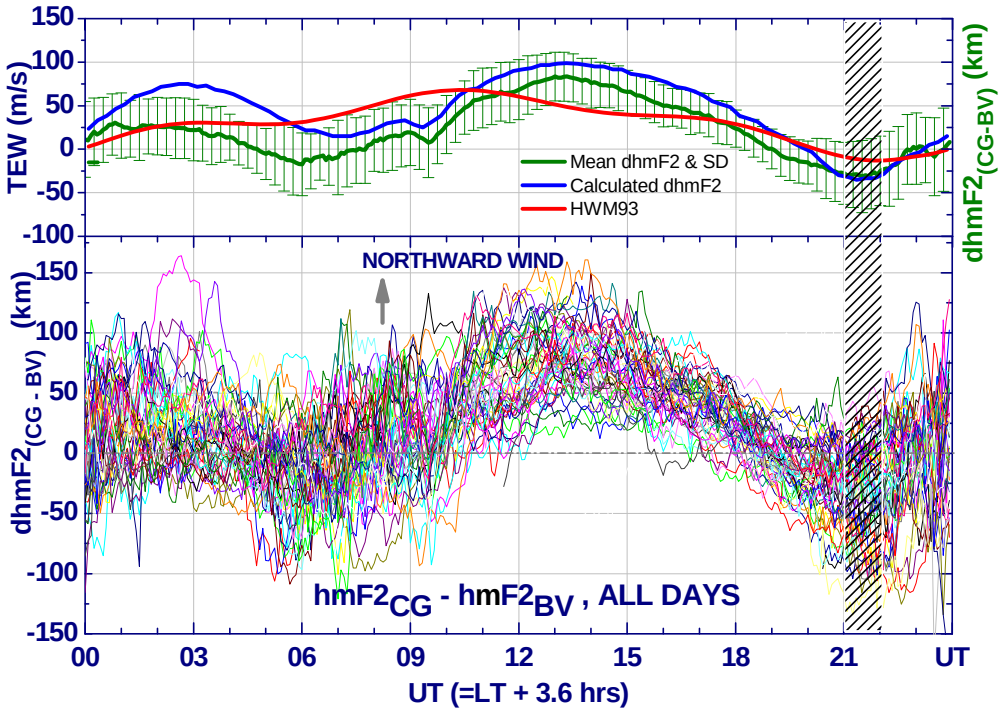

Fig.7

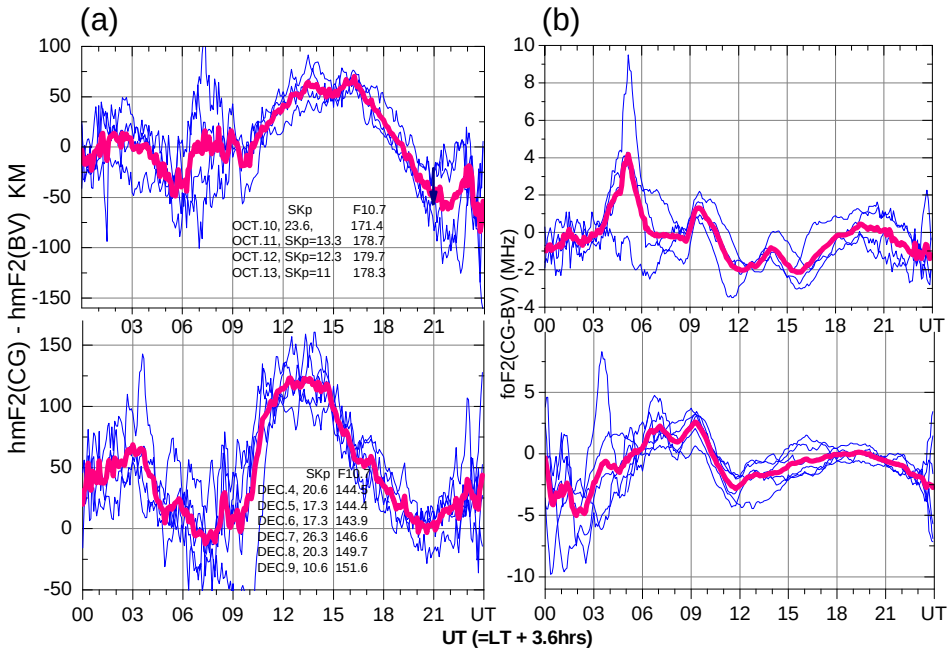
(a)
(b)
hmF2(CG) - hmF2(BV) KM
foF2(CG-BV) (MHz)
SKp F10.7
OCT.10, 23.6, 171.4
OCT.11, SKp=13.3 178.7
OCT.12, SKp=12.3 179.7
OCT.13, SKp=11 178.3
DEC.4, 20.6 144.9
DEC.5, 17.3 144.4
DEC.6, 17.3 143.9
DEC.7, 26.3 146.6
DEC.8, 20.3 149.7
DEC.9, 10.6 151.6
UT (=LT + 3.6hrs)

Fig. 8

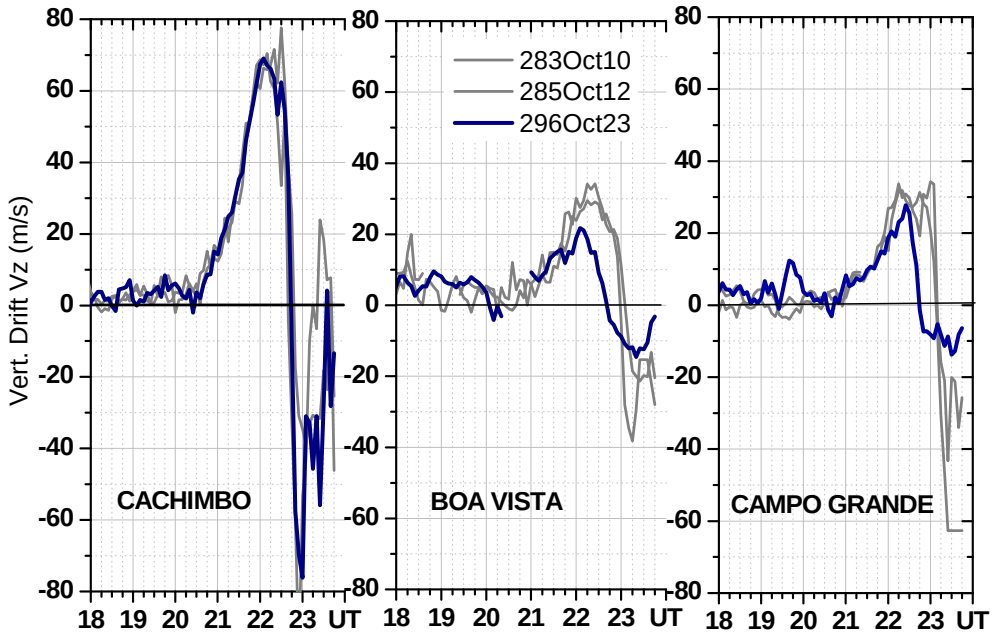
Vert. Drift Vz (m/s)
283Oct10
285Oct12
296Oct23
CACHIMBO
BOA VISTA
CAMPO GRANDE
UT

Fig. 9a

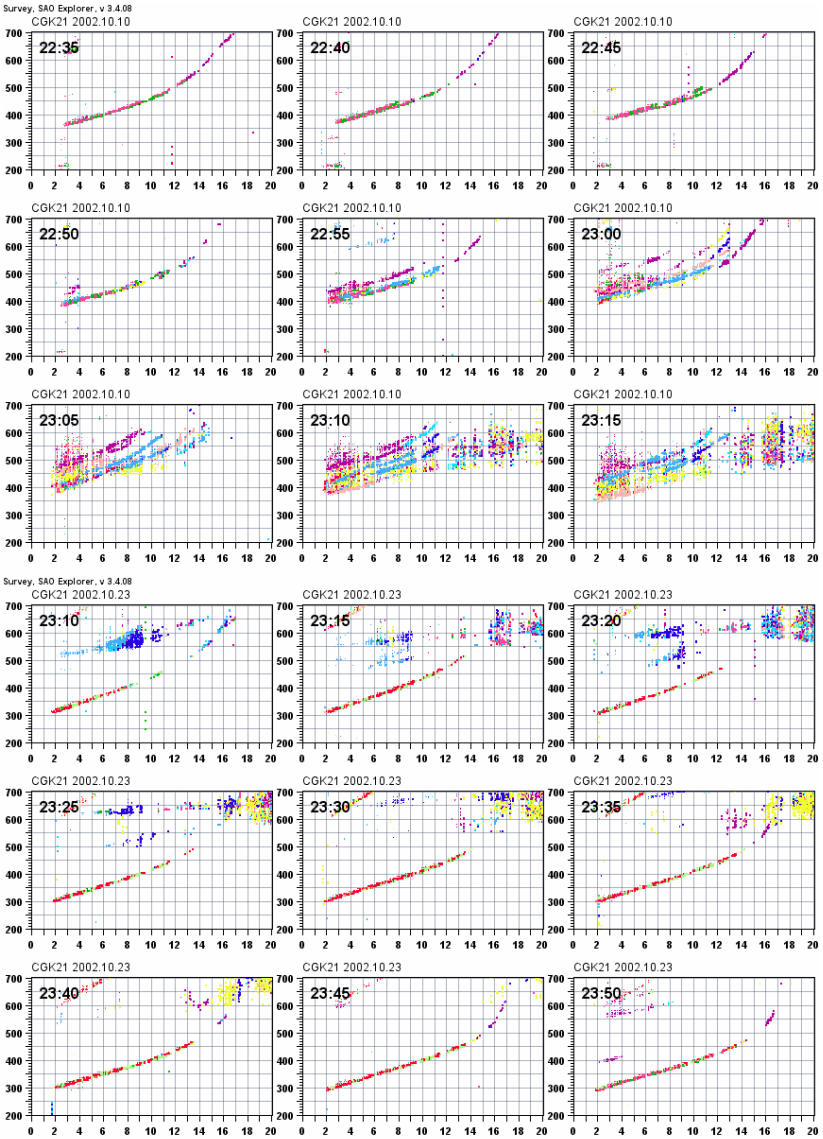
Survey, SAO Explorer, v 3.4.08
CGK21 2002.10.10
22:35
22:40
22:45
22:50
22:55
23:00
23:05
23:10
23:15
Survey, SAO Explorer, v 3.4.08
CGK21 2002.10.23
23:10
23:15
23:20
23:25
23:30
23:35
23:40
23:45
23:50

Fig.9b

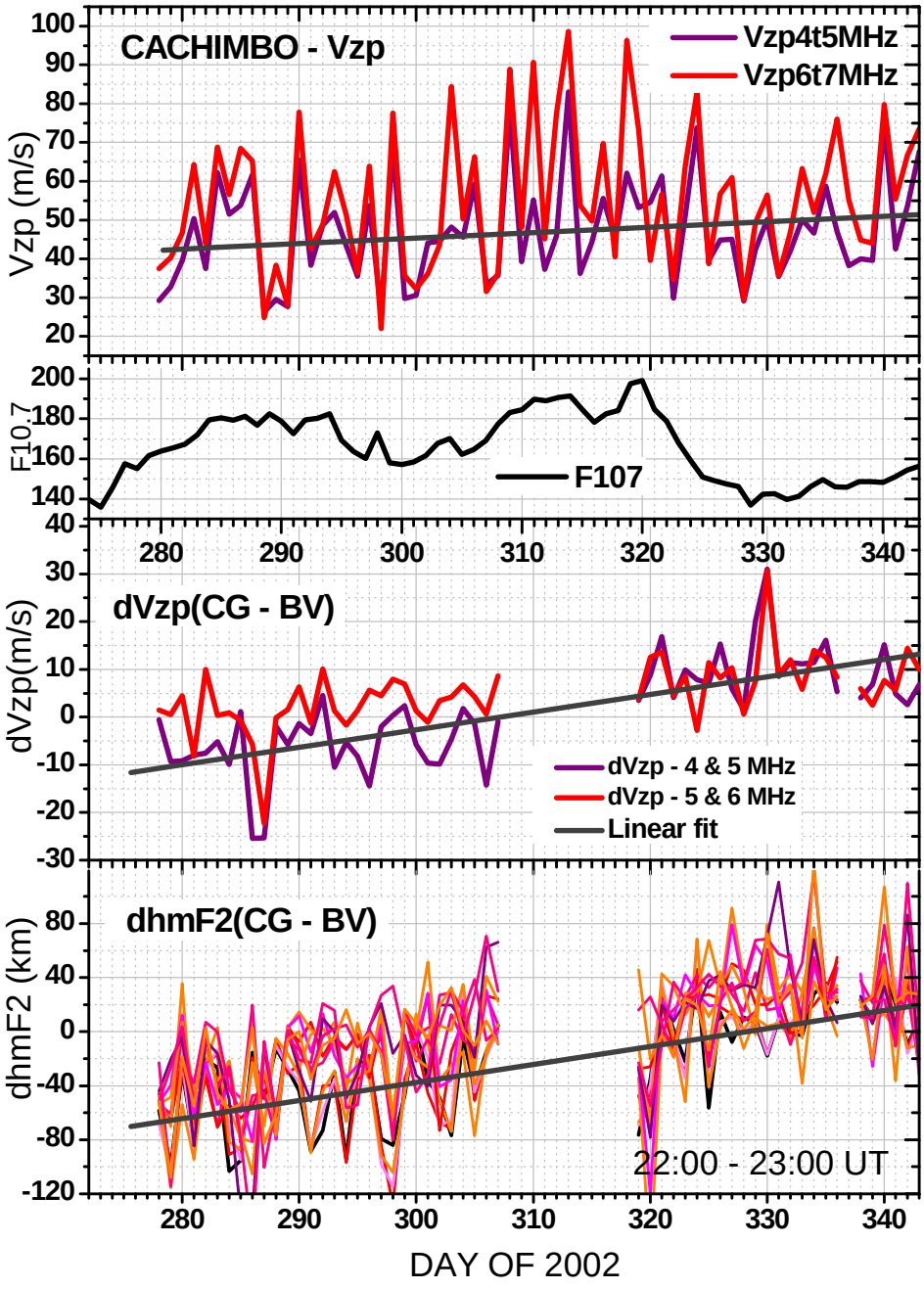
CACHIMBO - Vzp
Vzp4t5MHz
Vzp6t7MHz
Vzp (m/s)
F10.7
F107
dVzp(CG - BV)
dVzp(m/s)
dVzp - 4 & 5 MHz
dVzp - 5 & 6 MHz
Linear fit
dhmF2(CG - BV)
dhmF2 (km)
22:00 - 23:00 UT
DAY OF 2002

Fig. 10

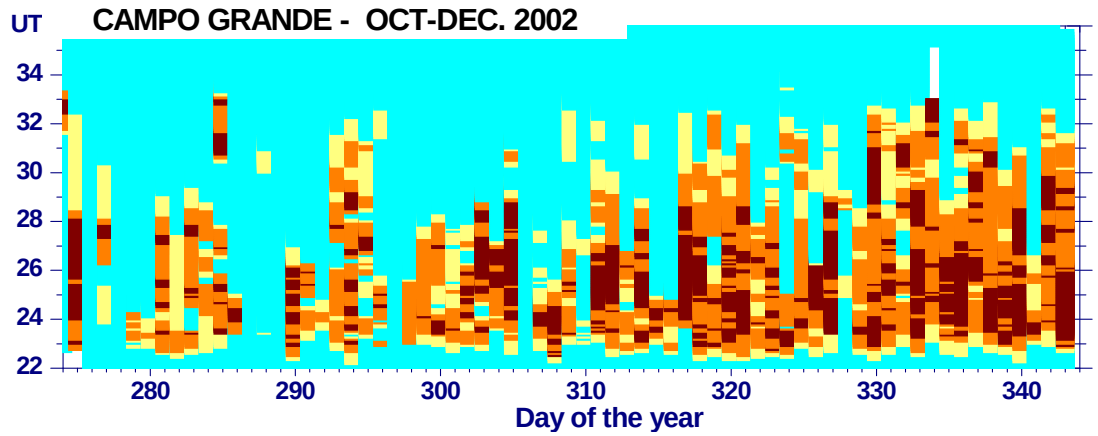
UT
CAMPO GRANDE - OCT-DEC. 2002
34
32
30
28
26
24
22
280
290
300
310
320
330
340
Day of the year

Fig. 11